Cortical gradients of functional connectivity are robust to state-dependent changes following sleep deprivation

NeuroImage 226 (2021) 117547

Contents lists available at ScienceDirect

NeuroImage

journal homepage: www.elsevier.com/locate/neuroimage

Cortical gradients of functional connectivity are robust to state-dependent changes following sleep deprivation

Nathan Cross[a,b,c,*], Casey Paquola[d], Florence B. Pomares[a,b,c], Aurore A. Perrault[a,b,c], Aude Jegou[a,e], Alex Nguyen[a,b], Umit Aydin[a,e,f], Boris C. Bernhardt[d], Christophe Grova[a,e,f,**], Thien Thanh Dang-Vu[a,b,c,*]

[a] PERFORM Centre, Concordia University, Montreal, Canada
[b] Center for Studies in Behavioral Neurobiology, Department of Health, Kinesiology and Applied Physiology, Concordia University, Montreal, Canada
[c] Institut Universitaire de Gériatrie de Montréal and CRIUGM, CIUSSS du Centre-Sud-de-l'Île-de-Montréal, Montreal, Canada
[d] Multimodal Imaging and Connectome Analysis Lab, McConnell Brain Imaging Centre, Montreal Neurological Institute and Hospital, McGill University, Montreal, Quebec, Canada
[e] Multimodal Functional Imaging lab, Department of Physics, Concordia University, Montreal, Canada
[f] Multimodal Funational Imaging Lab, Biomedical Engineering Dpt, Neurology and Neurosurgery Dpt, McGill University, Montreal, Quebec, Canada

A B S T R A C T

Sleep deprivation leads to significant impairments in cognitive performance and changes to the interactions between large scale cortical networks, yet the hierarchical organization of cortical activity across states is still being explored. We used functional magnetic resonance imaging to assess activations and connectivity during cognitive tasks in 20 healthy young adults, during three states: (i) following a normal night of sleep, (ii) following 24hr of total sleep deprivation, and (iii) after a morning recovery nap. Situating cortical activity during cognitive tasks along hierarchical organizing gradients based upon similarity of functional connectivity patterns, we found that regional variations in task-activations were captured by an axis differentiating areas involved in executive control from default mode regions and paralimbic cortex. After global signal regression, the range of functional differentiation along this axis at baseline was significantly related to decline in working memory performance (2-back task) following sleep deprivation, as well as the extent of recovery in performance following a nap. The relative positions of cortical regions within gradients did not significantly change across states, except for a lesser differentiation of the visual system and increased coupling of the posterior cingulate cortex with executive control areas after sleep deprivation. This was despite a widespread increase in the magnitude of functional connectivity across the cortex following sleep deprivation. Cortical gradients of functional differentiation thus appear relatively insensitive to state-dependent changes following sleep deprivation and recovery, suggesting that there are no large-scale changes in cortical functional organization across vigilance states. Certain features of particular gradient axes may be informative for the extent of decline in performance on more complex tasks following sleep deprivation, and could be beneficial over traditional voxel- or parcel-based approaches in identifying realtionships between state-dependent brain activity and behavior.

1. Introduction

The brain requires regular and recurrent sleep to maintain optimal functioning. While the precise reasons that explain the inevitable requirement for sleep are still being explored, the behavioural consequences of sleep deprivation (SD) are well-known and substantial. Acute total SD in particular has been observed to impair performance in cognitive domains such as visuomotor skills (Van Dongen et al., 2003), decision making (Blatter et al., 2005; Killgore et al., 2006; Linde et al., 1999), attention (Gevers et al., 2015; Kendall et al., 2006), logical reasoning (Drummond et al., 2004), fine motor skills (Ayalon and Friedman, 2008), and memory recall (Drummond et al., 2000; Forest and Godbout, 2000). However the most striking and replicated findings are impairments in vigilance (Doran et al., 2001; Muto et al., 2016; Drummond et al., 2005; Karakorpi et al., 2006; Rupp et al., 2012; Van Dongen et al., 2003; Yeo et al., 2015) and working memory (Chee et al., 2006; Choo et al., 2005; Forest and Godbout, 2000; Gevers et al., 2015; Lim et al., 2007; Rupp et al., 2012).

While studies have shown decreased task-evoked activations in regions of interest (ROIs) following SD, most commonly in fronto-parietal regions (Bell-McGinty et al., 2004; Chee and Tan, 2010; Chuah et al., 2006; Drummond et al., 2005, 2000; Lim et al., 2007; Muto et al., 2016; Tomasi et al., 2009), their magnitude have not always been predictive of behavioural impairment (Bell-McGinty et al., 2004; Lim et al., 2007). Additionally, increased activations have also been reported in other regions following SD (Bell-McGinty et al., 2004; Chee and Tan, 2010; Drummond et al., 2000; Tomasi et al., 2009). Indeed, task-evoked responses may display different patterns following SD depending on the task used and its difficulty, or the brain ROIs assessed. Thus, focusing on a dampening of specific task-evoked brain

* Corresponding authors at: PERFORM Centre, Concordia University, 7141 Sherbrooke St. West, SP 165.30, Montreal H4B 1R6, Canada.
** Corresponding authors at: Multimodal Functional Imaging lab, Department of Physics, Concordia University, Montreal, Canada.
E-mail addresses: nathan.cross@concordia.ca (N. Cross), christophe.grova@concordia.ca (C. Grova), tt.dangvu@concordia.ca (T.T. Dang-Vu).

https://doi.org/10.1016/j.neuroimage.2020.117547
Received 24 April 2020; Received in revised form 19 October 2020; Accepted 4 November 2020
Available online 11 November 2020

responses due to fatigue is unlikely to explain cognitive impairments in isolation.

Instead, the coordination of regions in large-scale networks, which can be non-invasively mapped using functional Magnetic Resonance Imaging (fMRI), may play a prominent role in determining the effects of prolonged wakefulness on cognitive function. However, few studies have attempted to bring into light associations between cognitive performance following sleep deprivation and functional connectivity, particularly during tasks. One study attempted to do so with seed-based functional connectivity but did not detect significant associations with behavior (De Havas et al., 2012). Later, other studies using resting-state functional connectivity detected that SD was associated with a loss of integration within large-scale functional networks and a reduced segregation between networks (Ben Simon et al., 2017; Yeo et al., 2015), as well as an increase in the fluctuation of the global signal (Wong et al., 2013; Yeo et al., 2015). These findings suggests that sleep deprivation may result in a reduction of order (i.e., increased entropy) in the brain. Importantly, in one of these studies subjects who were more resilient to lapses in vigilance following sleep deprivation exhibited a larger extent of highly segregated cortical networks, such as attention and default mode networks (DMN), when they were well rested (Yeo et al., 2015). This was only observed after accounting for the increase in the global signal fluctuation, however recent reports indicate that global signal regression (GSR) improves behavioral prediction accuracies taken from functional connectivity (Li et al., 2019a2019b). Nevertheless, this is supported by other findings showing that inter-individual differences in performance decline following sleep deprivation are trait-like (Dennis et al., 2017; Lim et al., 2007; Rupp et al., 2012; Van Dongen et al., 2003) and therefore may depend on individual characteristics of cortical organization.

Emerging analytical techniques that capture core axes of cortical organization open new avenues to explore individual differences related to extended wakefulness and resilience to sleep deprivation. These principle axes of variation in cortico-cortical functional connectivity are reflected in large-scale functional gradients, where the relative positioning of all cortical regions along a functional gradient inform upon the similarity of their connectivity profiles (i.e. the profile of their functional connectivity to all other cortical regions) and defined by maximally variant regions at either end (Margulies et al., 2016; Lariviere et al., 2020; Haak et al., 2018; Bethlehem et al., 2020; Paquola et al., 2019). Functional gradients, estimated using a multivariate statistical framework, provide a low-dimensional representation of global cortical organization of functional connectivity patterns. Moreover, although these gradients are decomposed from functional MRI data, they recapitulate hierarchical organization of information processing streams derived from invasive tract-tracing and histology (Margulies et al., 2016; Mesulam 1998; Paquola et al., 2019). Furthermore, those gradients are assumed to be important for constraining cognitive processes in the brain (for review, see (Huntenburg et al., 2018).

Alongside detailing patterns of activity in specific regions of interest during a cognitive task, probing the hierarchy of cortical function would serve to provide more comprehensive and detailed insight into impairments in behavior. In that context, cross-referencing task-related activations to their position along those functional gradients (Murphy et al., 2018; Murphy et al., 2019) can be used to demonstrate the core axes of functional organization that are relevant for the cognitive processes in question. Recent work demonstrating age-related individual differences in functional gradients are relevant for cognitive decline (Bethlehem et al., 2020), suggests that this framework may be optimally suited to probe the significant impacts of sleep deprivation on cognition.

Thus, the aims of this study are: 1) to identify which functional axes reflect brain activation patterns across cognitive tasks of attention, vigilance, and working memory; 2) to understand if, how, and to what extent these axes of functional organization change following SD and recover after an opportunity to nap, and; 3) determine whether individual characteristics of this organization might predict the impairments in cognition experienced following SD and their recovery after a nap.

We expect task activation patterns will adequately reveal that specific gradient axes are relevant for ongoing cognitive processes. Also, if functional gradients constitute an inherent coordinate system of the human cerebral cortex, then they will provide an opportunity to test the extent of disordered functional connectivity caused by sleep deprivation. It is unlikely however that this general organization will be severely distorted following sleep deprivation, because core cognitive processes are still achievable and individual traits are still noticeable. Based on previous findings that higher segregation of large-scale cortical networks at rest may be partially protective against the performance decline following sleep deprivation (Yeo et al., 2015), and that the technique of situating cortical activity in a gradient space attempts to highlight the extent of differentiatied brain regions, it was hypothesised that the range (distance from one end to the other) of certain gradient distributions, or the dispersion of networks within this gradient space, may result in effective low-dimensional predictors of resilience to state-dependent changes in cognition, such as following sleep deprivation.

Finally, given the debate around the use of GSR in functional connectivity analyses, and the fact that previous results looking at these analyses after sleep deprivation reported significant results only after GSR, we performed our analyses both without and with GSR. This allowed us to explore the effects of GSR on gradient distribution, their state-dependent changes, and the relationship with performance.

2. Methods

2.1. Participants

Participants were recruited using advertisements posted online and within Concordia University, Montreal. A semi-structured interview was conducted to assess their eligibility. Participants were required to be aged between 18 and 30 years and considered good sleepers (>6 h of sleep per night) with an absence of any sleep disorders (participants with insomnia, sleep apnea syndrome with an apnea-hypopnea index >5/hr, central disorders of hypersomnolence, restless legs syndrome, periodic limb movements during sleep with an index >15/hr, and parasomnias were excluded). Participants were also excluded for neurological or psychiatric conditions (e.g. epilepsy, migraine, stroke, chronic pain, major depression, anxiety disorder, psychotic disorder) and current use of psychotropic medications or cannabis. Subjects were also asked to refrain from smoking tobacco for the entire duration of the study. All subjects provided informed consent prior to the start of the study that was approved by the Central Research Ethics Committee of the Quebec Ministry of Health and Social Services.

2.2. Study procedure

The study protocol is outlined in Fig. 1A. Participants made three visits to the laboratory. On the first visit, they were briefed on the study protocol and completed an overnight polysomnography to adapt to the environment and to screen for any sleep disorders. To monitor their sleep pattern between this visit and the remaining visits, each participant was given a wrist actiwatch (Actiwatch, Philips Respironics, USA) that had to be worn until they completed the experiment. Only subjects with a good sleep habit (slept for > 6 hr per night with a consistent schedule) were invited to participate in the subsequent sessions.

The second and third visits were well-rested (WR) or sleep deprivation (SD) sessions. The WR and SD sessions were separated by a minimum of one week and the order of test sessions was counterbalanced across participants. During the WR session, participants arrived at 7:00pm and were given a 9-hour sleep opportunity in a dark, quiet room. During the SD session, participants arrived at 8:00 pm and stayed awake the entire night in the laboratory. They were free to do as they wish, but were constantly monitored and prevented from consuming

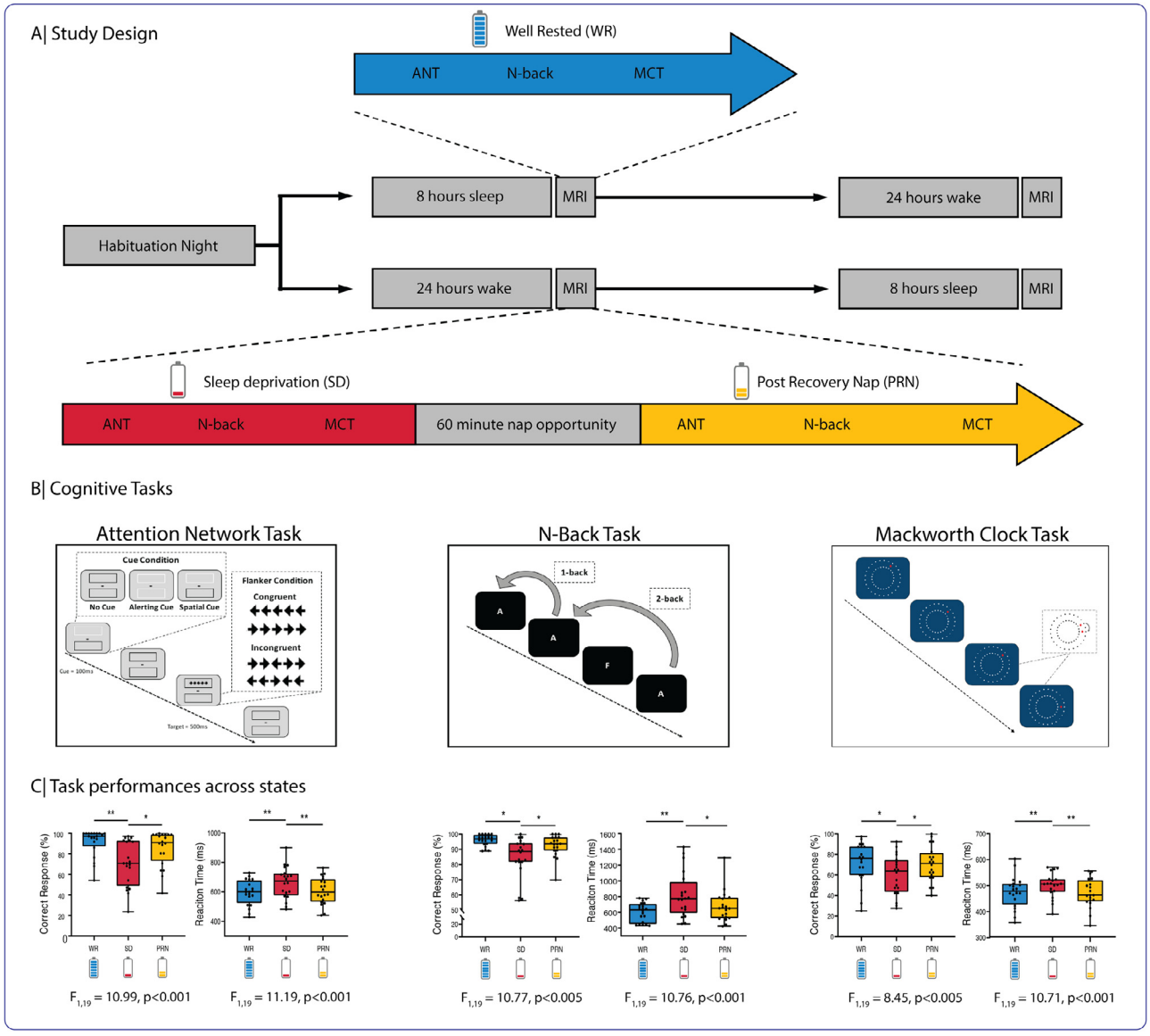

Fig. 1. Study design and behavioural results. **A.** Participants made 3 visits to the lab: a habituation night, followed by a counterweighted design of either another full-night opportunity to sleep (blue), or a night of total sleep deprivation. In the morning following each night, participants completed cognitive tasks inside the MRI scanner. In the sleep deprived state (red), participants also had a recovery nap opportunity (yellow) and then recompleted the tasks inside the MRI scanner. **B.** The cognitive tasks encompassed domains that have been shown impaired following sleep deprivation: Attention - the Attention Network Task (Fan et al., 2002); Working memory - the N-back Task (Kirchner 1958); and Vigilance - the Mackworth Clock Task (Lichstein et al., 2000). **C.** The percentage of correct responses and mean reaction time on all tasks was significantly impaired following sleep deprivation, and improved following a recovery nap.

any stimulants or performing anything too stimulating (e.g. exercising or watching horror films). Light levels were set at a constant level for all subjects throughout the entire night.

In both sessions, subjects were taken to the MRI at 7:00am to be prepared for scanning, including the application of an MRI compatible high-density EEG cap for objective monitoring of wakefulness. Scanning began at 8:00am. In the WR state, the session involved two resting state sequences (a fixation cross (5 min) and the Inscapes video (7 min); Vanderwal et al., 2015), followed by three cognitive tasks: the Attentional Network Task (ANT), the N-back task, and the MCT; an anatomical T1w scan, and a diffusion weighted imaging scan. In the SD state, the first session also involved the same two resting state sequences, followed by the three cognitive tasks. Then subjects were provided a 60-minute nap opportunity inside the MRI scanner. After 60 min, the participant was woken and during the final session (post recovery nap, PRN), subjects recompleted all of the cognitive tasks, as well as one resting state sequence (fixation cross). At the completion of the study, subjects were debriefed and were advised not to drive home if they had just completed the SD session.

2.3. Cognitive tasks and other sequences

The cognitive tasks (Fig. 1B) were chosen to reflect different types of cognitive processing due to the known sigificant effects of sleep deprivation in these cognitive domains:

Mackworth Clock Task: The version of this vigilance task used in this study consisted of a circular stimuli presented on screen spatially similar to a ticking clock. A node sequentially traversed the circumference of the circle in discrete steps. The participants were asked to press the trigger when the stimuli skipped or 'jumped' a step (Lichstein et al., 2000; Loh et al., 2004). The task lasted 5 min in duration, with each

block lasting 18 s and rest period between blocks was 15 s. Therefore, this task resembles a simple attention task.

Attentional Network Task (ANT): This task probes different attentional processes, such as alerting, orienting and executive control (Fan et al., 2005, 2002). The ANT consists of a series of trials in which the participant is required to identify the direction (left or right) of the middle arrow in an array of five arrows within an upper or lower panel of the screen. The arrow is either congruent or incongruent to the direction of all other arrows. Different cues are displayed immediately prior to the appearance of the arrows, including both panels flashing (double cue; alerting), or either panel flashing (valid or invalid cues; orienting). For a subset of trials, no cue precedes the appearance of the arrows (no cue). The ANT lasted 13 min in duration, with each trial lasting 1 s with a random jitter (range = 2–12, mean = 5 s) between each trial.

N-back task: This working memory task consisted of a sequence of letters presented one at a time in the center of the screen (Kirchner 1958; Sweet 2011). The participant was required to respond depending on the difficulty level of each block of trials. At level 0-back, the participant responded on every trial in the block. This served as a control condition for investigating activations related to higher level processing. At level 1-back, the participant responded whenever the letter of two subsequent trial was the same. At level 2-back, the participant responded whenever the letter presented was the same as the letter presented 2 trials previously. The N-back lasted 8 min in duration, with each block lasting 38 s with 10 s between each trial.

All tasks were run on a laptop computer using Inquisit software (Millisecond Software LLC, 1998), displayed to the participant via a projector screen behind the MRI scanner. The participant responded to all tasks via button presses made using a response pad attached to the fingers of the left hand. For all tasks, outcomes of reaction time (ms), accuracy (%; correct trials/number of trials), and lapses (number of missed responses) were measured.

2.4. Monitoring of wakefulness and sleep

Participants were monitored for wakefulness during scanning through a live video recording of the eyes. They were given a wake-up call if their eyes were closed for more than 10 s during the resting-state or cognitive tasks to prevent them from falling asleep. When there was uncertainty surrounding wakefulness inside the scanner, post-hoc confirmation of wakefulness and sleep was verified using the electroencephalography (EEG) that was acquired simultaneously.

2.5. EEG acquisition and preprocessing and scoring

EEG was acquired using an MR compatible 256 high-density geodesic sensor EEG array (Electrical Geodesics Inc (*EGI),* now *Philips Neuro, Oregon USA*). The EEG cap included 256 sponge electrodes referenced to Cz that covered the entire scalp and part of the face. EEG data were recorded using a battery-powered MR-compatible 256-channel amplifier shielded from the MR environment that was placed next to the participant inside the scanning room. The impedance of the electrodes were initally maintained below 20kΩ and kept to a maximum of 70kΩ throughout the recording. Data were sampled at 1000 Hz and transferred outside the scanner room through fiber-optic cables to a computer running the Netstation software (*v5, EGI*). The recording of EEG was phase-synchronized to the MR scanner clock (*Sync Clock box, EGI*), and all scanner repetition times (TRs) and participant responses were recorded in the EEG traces. Electrocardiography (ECG) was also collected via two MR compatible electrodes placed between the 5th and 7th ribs and above the heart close to the sternum, and recorded at 1000 Hz through a bipolar amplifier (*Physiobox, EGI*).

The EEG data were preprocessed using the Brainvision Analyzer (*Brain Products Inc, Gilching Germany*). Firstly, the EEG data were corrected for MR gradient artefacts using a 21 s sliding window template. Ballistocardiographic pulse-related artefacts were separated from the signal using a template time-locked to the detected QRS peaks in the ECG channel and then removed from the EEG signal. The MR-denoised EEG signal was bandpass filtered between 1 and 20 Hz to remove low-frequency drift and high-frequency noise, down-sampled to 250 Hz, and re-referenced to the linked mastoids.

The task- and resting-wake EEG recordings were scored post-hoc to confirm participant wakefulness during these sessions. Scoring of the sleep session was performed in conjunction by two trained scorers (NC & AP) using the wonambi toolbox (https://github.com/wonambi-python/wonambi) (using the channels Fz, F3, F4, C3, C4, O1 and O2) in order to obtain measures of sleep including total sleep time, and the duration of sleep stages.

2.6. MRI acquisition

MRI scanning was acquired with a 3T GE scanner (General Electric Medical Systems, Wisconsin, US) using an 8-channel head coil. Functional scans were all acquired using a gradient-echo echo-planar imaging (EPI) sequence (TR = 2500 ms, TE = 26 ms, FA = 90°, 41 transverse slices, 4-mm slice thickness with a 0% inter-slice gap, FOV = 192 × 192 mm, voxel size = 4 × 4 × 4mm^3 and matrix size = 64 × 64). High-resolution T1-weighted structural images were acquired using a 3D BRAVO sequence (TR = 7908 ms, TI = 450 ms, TE = 3.06 ms, FA = 12°, 200 slices, voxel size = 1.0 × 1.0 × 1.0 mm, FOV = 256 × 256 mm).

During all EEG-fMRI sessions, the helium pump was switched off in order to reduce noise artefacts infiltrating the EEG signal. To minimize movement-related artefacts during the scaning, MRI-compatible foam cushions were used to fix the participant's head in the head coil.

2.7. MRI preprocessing

Preprocessing of fMRI data was performed using fMRIPrep 1.3.1 (Esteban et al., 2019); RRID:SCR_016216), which is based on Nipype 1.1.9 (Esteban et al., 2020; Gorgolewski et al., 2011); RRID:SCR_002502). Firstly, the T1-weighted (T1w) image was corrected for intensity non-uniformity (*ANTs v2.2.0*) and used as T1w-reference throughout the workflow. Then a reference volume of the EPI image and its skull-stripped version were generated using a custom methodology of fMRIPrep. The BOLD reference was then co-registered to the T1w reference using bbregister (*FreeSurfer v6.0*) which implements boundary-based registration (Greve and Fischl, 2009). Co-registration was configured with nine degrees of freedom to account for distortions remaining in the BOLD reference. Head-motion parameters with respect to the BOLD reference (transformation matrices, and six corresponding rotation and translation parameters) were estimated (*mcflirt, FSL v5.0.9*; (Jenkinson et al., 2002) before slice-timing correction (*AFNI*, (Cox, 1996)). The BOLD time-series (including slice-timing correction when applied) were resampled onto their original, native space by applying a single, composite transform to correct for head-motion and susceptibility distortions. Transforms are concatenated and applied all at once, with one interpolation (Lanczos) step, so as little information is lost as possible. Frame Displacement and the spatial standard deviation of successive difference images (DVARS) were calculated for each functional run, both using their implementations in Nipype. Brain tissue segmentation of cerebrospinal fluid (CSF), white-matter (WM) and gray-matter (GM) was performed on the brain-extracted T1w using FAST (*FSL v5.0.9*, RRID:SCR_002823, (Zhang et al., 2001). The average timeseries of the cerebrospinal fluid (CSF), white matter (WM), and whole-brain were also extracted. After sampling the BOLD time-series onto their original, native space, these were then resampled via nonlinear transformation to the MNI152NLin2009cAsym standard volumetric space for all subjects for subsequent processing and analysis, keeping the original resolution of the BOLD data.

The BOLD data timeseries in standard space were further denoised using a 36-parameter stream of the xcpEngine (Ciric et al., 2017). First,

a temporal filter (0.01–0.08 Hz) was applied to the data. Then, six realignment parameters, the mean WM and CSF time series (extracted from fMRIPrep), as well as derivative and quadratic expansions, were all regressed out from the BOLD timeseries. The residuals were kept as processed data for subsequent analyses. Due to previous reports of the significant increase in global signal following sleep deprivation and reduced arousal levels (Ben Simon et al., 2017; Wong et al., 2013; Yeo et al., 2015), preceding steps were repeated with and without global signal regression (GSR).

The final preprocessed BOLD time series for each subject was projected onto the cortical surface (white matter boundary, default) using the fsaverage5 template from the Freesurfer package (*mri_vol2surf; FreeSurfer v6.0*), and smoothed along the surface space using a 6 mm smoothing kernel. The BOLD timeseries for each vertex on the fsaverage surface was then assigned to one of 400 cortical parcels from a predetermined standardised template of functionally similar cotical regions (Schaefer et al., 2018), where each parcellation is also assigned to one of 17 functional resting state networks (Yeo et al., 2011). The timeseries for all the vertices corresponding to each parcel were averaged to give one mean timeseries per parcel, resulting in a total of 400 timeseries across both cortical hemispheres.

All MRI preprocessing was performed on the Compute Canada servers Cedar and Graham (https://www.computecanada.ca/research-portal/accessing-resources/available-resources/).

2.8. Task activations

The timing of each stimulus and participant response for all tasks were obtained from the Inquisit output files and EGI marker files. These times were modeled with a finite impulse response to transform them into a timeseries. The modelled task timeseries was downsampled to match the TR sampling rate (0.4 Hz), and convolved with a hemodynamic response function (*canonical HRF; SPM 12*), for the HRF only but no derivatives. The timeseries was then entered into a design matrix. The matrix formulation allowed for the calculation of the least square fit for the line:

$$\boldsymbol{Y} = \boldsymbol{X} * \boldsymbol{B} + \boldsymbol{E}$$

Where **Y** is the data matrix, **X** is the design matrix (each condition per task and a constant), **B** is the parameter matrix (the beta and the y-intercept of the regressor, denoted as a constant **C**), and **E** is the error matrix (residuals). This is the statistical formula for a simple regression that most major neuroimaging pipelines implement, and follows the assumption that the BOLD data at timepoint ***t*** comprise of a linear effect of **X** (beta $*$ $\mathbf{X}_t$ + **C**) and random fluctuations ($\mathbf{E}_t$).

To calculate activations specific to task related performance (i.e. to express hypotheses about the effects defined by the design matrix) a contrast weights vector was created, which when multiplied by **B**, returned the numerator of the t-statistic of comparing task-conditions. The contrasts vectors were designed specifically for each task. For the MCT, a block design was implemented, such that activity during the task-blocks was compared to the null hypothesis. For the N-back task, a block design was also implemented. Activations for blocks of 0-back, 1-back and 2-back were calculated against the null-hypothesis, then contrasted between the 0-back and 1- and 2-back task-condition blocks. As a condition for working memory, only the 2-back vs. 0-back contrast was included in these analyses. For the ANT, a trial design was used. Activations for each task-cue (no cue, alerting cue, orienting cue) were modelled separately and compared to the null hypothesis to obtain a general activation during the entire task.

The BOLD timeseries was modelled with the design matrix for each of the 400 cortical parcels separately, for each subject, at the first level. At the second level, each of the 400 modelled beta statistics across subjects for each of the experimental-conditions (WR, SD and RN) were compared to the null hypothesis, and also contrasted against each other (i.e. WR vs SD, SD vs RN). The significance at the second level was set at $p < 0.05$, and corrected for multiple comparisons using a false-discovery rate (FDR) method (Benjamini and Hochberg, 1995). A repeated measures linear model was applied to assess changes in activations between the 3 states (WR, SD, PRN), FDR corrected across the 400 parcels, followed by pos-hoc t-tests to detect specific state-level changes.

2.9. Functional connectivity analysis

For each subject and session, the preprocessed BOLD timeseries were first concatenated across all tasks, as previously implemented for studying the underlying core of general cognitive processing in the human brain (Elliott et al., 2019; Shine et al., 2019; Zhu et al., 2017). The general HRF task-specific activity (i.e. for all trials for the ANT and all blocks for the MCT and N-back tasks) was regressed out from the BOLD timeseries to reduce the influence of task-evoked coactivation in the connectivity analyses (De Havas et al., 2012; Wang et al., 2016). Such an approach has been shown to be comparable to resting state functional connectivity studies and used to extract information about the intrinsic properties of cortical connectivity (Elliott et al., 2019). Task-based sequences were used over resting-state sequences because: 1) several subjects fell asleep during the SD resting-state session; 2) the use of concatenated task sequences provided a much longer timeseries (23 min vs 5 min) allowing for greater spatial dimensionality (400 parcels) and more consistent gradients, and; 3) because the extracted BOLD timeseries reflects the brain state at the time of the task performances. Nevertheless, consistent with previous studies, in the WR state, the task-regressed correlation matrix was actually significantly correlated with the resting state correlation matrix ($r = 0.91$, $p<0.001$). The resulting resampled BOLD timeseries were finally correlated between all 400 parcellations, resulting in a 400 × 400 correlation matrix, with 79,800 (= 400 × 399 / 2) unique Pearson's correlation values. A Fisher's r-to-z transformation was applied to the correlation values to encourage normality prior to the transformation of functional connectivity into cortical gradients of functional similarity.

2.10. Generation of functional gradients and comparison with task activation patterns

Baseline functional gradients were first derived from the group-average functional connectivity matrix estimated from the WR session. Following methodology used previously (Bethlehem et al., 2020; Margulies et al., 2016; Lariviere et al., 2020; Paquola et al., 2019), the functional connectivity matrix was proportionally thresholded at 90% per row, then the similarity of regional connectivity profiles were calculated using row-rise cosine similarity (to ensure symmetry) and rescaled to 0.5–1 (to ensure non-negative values). This normalised angle matrix was then subjected to diffusion map embedding, a non-linear dimensionality reduction technique (Lafon et al., 2006; Vos de Wael et al., 2020). In this new space, cortical nodes that are strongly interconnected by either many suprathreshold edges or few very strong edges are closer together, whereas nodes with little or no intercovariance are farther apart. With diffusion map embedding, a random walker is initialised to approximate the likelihood of transition between nodes, illuminating the local geometry of the normalised angle matrix. The name of this approach, which belongs to the family of graph Laplacians, derives from the equivalence of the distance between points in the low-dimensional embedding space and the diffusion distance between probability distributions at those points. The form of the input matrix, which is subjected to 90% row-wise thresholding and row-rise cosine normalization of edges between 0.5 and 1, reduces the likelihood of outlier regions. Outliers weren't observed in the projection. This results in a transition matrix, across which a Markov chain is run forward in time linking the local geometries into a set of global axes. These global axes are represented as a set of eigenvectors of the diffusion map embedding, commonly referred to as gradients in neuroimaging practice. All cortical parcels could thus be projected on each gradient. The relative value of regions projected

along a functional gradient inform upon the similarity of their functional connectivity profiles (i.e. normalized connectivity profile with all other cortical regions), in relation to that axis of cortical organistion. Each gradient can be described by its anchor points – i.e. the regions that are projected at each extreme end of the gradient, and which have therefore maximally variant functional connectivity profiles. Regions in the center of a gradient express functional connectivity profiles that are less distinguishable. The first three gradients were selected for subsequent analysis, as they account for approximately 50% of the total variance and have been previously well characterised (Bethlehem et al., 2020; Margulies et al., 2016). The above was repeated for the group average connectivity matrices in the SD and PRN conditions, which were then aligned to the baseline (WR) functional gradients via Procrustes rotation (Langs et al., 2015; Wang and Mahadevan, 2008).

To compare task activations patterns to the functional gradients, once the 400 parcellations were arranged along a gradient, they were then discretized (i.e., grouped) into 50 equally sized bins (i.e., spatial clusters across the entire gradient), following a recent approach to stratify task-based fMRI data using connectome topographies (Murphy et al., 2018; Murphy et al., 2019). This was performed for each gradient separately. In each subject, t-statistics task-activations (per task) were then averaged within each bin, and values were smoothed with a 10-bin Gaussian kernel. T-statistic values within each bin were then contrasted between states at a second level and corrected for multiple comparisons using a FDR of $p<0.05$.

2.11. Distance metrics in the functional gradient space

Gradients were also calculated (using the same diffusion map embedding procedure as described above) from the connectivity matrix for each individual in each three states. Individual functional connectivity matrices from the SD and PRN sessions were then aligned to their baseline (WR) individual functional gradients via Procrustes rotation. To estimate the impact of sleep deprivation and a recovery nap on segregation of cortical function, we calculated a set of measures to quantify the dispersion within and between functional communities in a multi-dimensional connectivity space, bounded by all three gradients simultaneously. These measures were: (i) the numerical range of each functional gradient; (ii) the centrality of all cortical parcels in this 3D space; (iii) the dispersion of functional networks (Yeo et al., 2011) in the 3D gradient space, and; (iv) the pairwise Euclidean distance between all cortical parcels in the 3D gradient space. Specifically, the range of each gradient was calculated as the distance from the minimum to the maximum gradient eigenvector values, and indicates a segregation (i.e. different conectivity profile) of the gradient extremes as well as an increased connectivity pattern within the extremes. For each parcel, centrality was calculated as the average Euclidean distance to all other parcels in the 3D gradient space (accounting for the full 3D space and not one gradient only). In this context, high centrality refers to the smallest distance to all other parcels in space (i.e. towards the center of the 3D gradient space), and thus indicates a functional connectivity profile that isn't differentiated across all three gradients. Within-network dispersion was calculated as the sum of the squared Euclidean distances in the 3D gradient space of all parcels within that network to the network centroid (i.e., the mean coordinates in 3D gradient space of all parcels belonging to that network). A small dispersion value could be interpreted as a highly integrated network, segregated from other networks. These multi-dimensional gradient metrics are motivated by prior related work on network integration and segregation, are assumed to reflect segregation of functional networks, and have been demonstrated to be comparable with other approaches of measuring network changes such as clustering, as well as within-network connectivity and segregation (Bethlehem et al., 2020). Particularly, Euclidean distance in the 3D gradient space reflects the similarity of connectivity profiles between cortical parcellations, across multiple axes of differentiation. The metrics were compared across states (WR, SD and PRN) using a repeated-measures linear model with post-hoc t-tests between states. Finally, the range of gradients were compared before and after applying GSR with paired-sample t-tests $p<0.05$.

2.12. Comparisons of cognitive performances across states

To compare cognitive performances across the three states we first performed a repeated measures ANOVA to check for the effect of state. Then a Tukey's post-hoc (q) test was used to compare performances between each state, which controls for multiple comparisons.

2.13. Prediction of state dependent changes in cognitive performance with functional connectivity during the well-rested state

We aimed to test the predictive utility of vulnerability to sleep deprivation and the recovery following a nap using the distance metrics of the three gradients. Firstly, the ranges of each gradient at the WR state were together entered into stepwise linear regression models as predictors. Then, the change in accuracy of correct responses from WR to SD (as% of score in the WR sate) and from SD to PRN on the MCT, ANT and 2-back were entered separately as dependent variables, resulting in 6 stepwise regression models. In each, starting from a constant model, a forward and backward stepwise regression was used to determine a final model. The initial model contained an intercept, linear term for each predictor, and all products of pairs of distinct predictors (no squared terms).

To assess the relationship between cognition and measures of network dispersion in the 3D gradient space (i.e. network level segregation), we used a partial least squares (PLS) model. This was chosen over a linear regression model due to a) the number of predictors, and b) the high collinearity between network dispersion metrics making them unsuitable for multiple linear regression. PLS analysis is a multivariate statistical technique that finds weighted patterns of variables in a predictor set (X) and response set (Y) to achieve maximum covariance across all variables (Krishnan et al., 2011; McIntosh and Lobaugh, 2004; McIntosh and Misic, 2013). We entered the range of the 3 gradients and dispersions of 17 functional networks in 3D gradient space into a Nx20 matrix $\mathbf{X}$ and the cognitive measures at the WR state (RT and accuracy for all three tasks) into a Nx6 matrix $\mathbf{Y}$ (where N is the number of subjects). A covariance matrix was created from these two variable sets and subjected to singular value decomposition (Eckart and Young, 1936):

$$\mathbf{X}^{\mathrm{T}}\mathbf{Y} = \mathbf{U}\Delta\mathbf{V}^{\mathbf{T}}$$

to identify latent gradient-cognition variables $\mathbf{U}$ and $\mathbf{V}$, where $\mathbf{U}$ and $\mathbf{V}$ are matrices of left (predictor) and right (response) singular vectors, and $\boldsymbol{\Delta}$ is a diagonal matrix with singular values along the diagonal.

Statistical significance of these resulting latent variables (i.e. their predicitive utility) was assessed by 10,000 permutations, determining how these latent variables compared to a null distribution of singular values. Permutation tests were conducted by randomly reordering the rows of the original data matrix $\mathbf{X}$, generating a set of permuted data matrices where the original ordering of individual participants had been shuffled. The reliability of singular weights (i.e., weights of specific network dispersion variables) were assessed using bootstrap resampling (10,000 repetitions), which was performed by randomly resampling participants with replacement (i.e., the rows of data matrices $\mathbf{X}$ and $\mathbf{Y}$). This allowed patterns derived from the analysis to be cross-validated. Bootstrap ratios were calculated as the ratio of each variable's weight to its bootstrap-estimated standard error, as has been employed in other studies (Kirschner et al., 2020; Mišić et al., 2016). We first performed the PLS analysis with just the performance measures at the WR state, to determine if these network dispersion metrics in gradient space were relevant for cognition generally. This was repeated for the change in cognitive measures from the WR to the SD state, as well as from SD to PRN, to determine whether dispersion of networks informs state-dependent changes in cognitive performance.

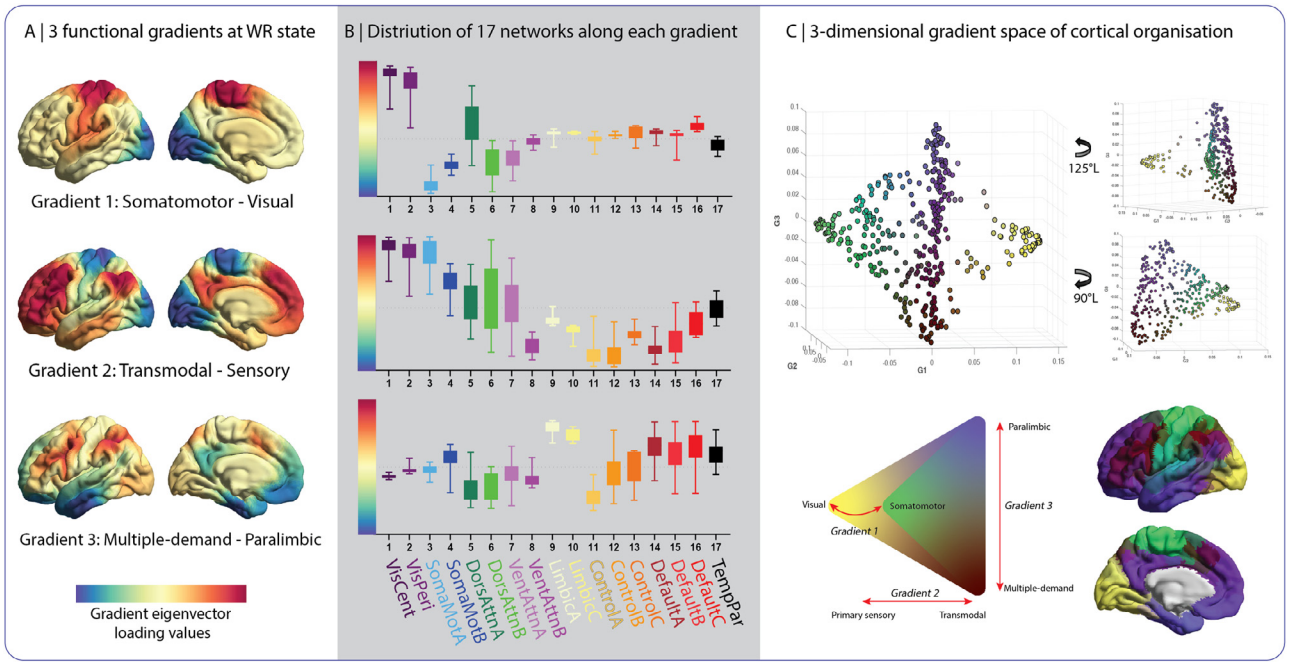

Fig. 2. Cortical gradients of functional organization. **A.** The topographic profile of each gradient along the cortex. **B.** The distribution of gradient eigenvector loading values (boxplot representation) for parcels belonging to the 17 functional networks (Yeo et al., 2011) along each gradient demonstrates the clear distinction of somatomotor to visual regions in gradient one, transmodal to sensory regions in gradient two, and multiple-demand to paralimbic regions in gradient three. The y-axes are in arbitrary units, however are the same scale across the three gradients. **C.** The three gradients projected in a 3-dimensional gradient space, with rotations of the space for visualization. This axes of this 3D space represent each gradient, and separate distinct functional poles of cortical organization. When the three gradient axes are projected simultaneously onto the cortical surface, they show an organised spatial pattern.

2.14. Code and data availability

All code used in this manuscript is available from https://github.com/nathanecross/sleep-deprivation/tree/master/Gradients

3. Results

Thirty-four participants were recruited for the study. Six participants were excluded due to the presence of sleep disorders (sleep apnea syndrome, restless legs syndrome) during the habituation night, 1 subject was excluded due to excessive motion and 1 due to artefacts during scanning, and six withdrew before the completion of the study. During the SD session, all participants included in the final sample remained awake throughout the tasks. Only one subject consistently dozed during cognitive testing, and this subject was removed from the final analyses due to excessive head motion artefact caused by dozing (0.58 mm average, compared to a group average of 0.19 ± 0.09 mm). The final sample consisted of twenty participants (mean age of 21.2 ± 2.5 years, 12 females). Average framewise displacement was not significantly different between the three sessions ($F = 2.36$, $p = 0.109$).

3.1. Task-related brain activation patterns across cortical gradients during rested wakefulness

Fig. 2 depicts three large-scale gradients that explained ~50% of the variance in the task-regressed functional connectivity matrices across the cortex. The first axis (gradient 1) depicts a gradient running from the somatomotor cortex to the visual areas (18.3% of variance explained). The second axis (gradient 2) depicts a gradient ranging from the transmodal cortex (Mesulam 1994) (e.g. frontoparietal and DMN) to the unimodal primary sensory areas (visual and somatosensory) (16.5% variance). The final axis (gradient 3) depicts a gradient running from areas commonly implicated in multiple-demands (executive control) to the paralimbic cortex (overlapping with part of the DMN) (13.5%). These gradients are in agreement with what have been reported previously in the literature (Bethlehem et al., 2020; Margulies et al., 2016; Paquola et al., 2019; Vos de Wael et al., 2020).

Activation patterns during the MCT were the most widespread of the 3 tasks (Fig. 3A). The largest magnitude activations were observed in the left and right frontal eye fields (5 parcels, $t = 6.6–9.1$, all $p<0.001$ FDR corrected), left and right superior parietal lobule (13 parcels, $t = 5.3–7.8$, $p = 0.001–0.004$ FDR corrected), left and right inferior parietal sulcus (8 parcels, $t = 3.6–5.0$, $p = 0.006–0.025$ FDR corrected), left and right extrastriate cortex (11 parcels, $t = 3.4–5.2$, $p = 0.003–0.035$ FDR corrected), and the left and front medial frontal gyrus (6 parcels, $t = 4.0–9.3$, $p = 0.001–0.025$ FDR corrected). There were also significant deactivations within the left and right superior extrastriate cortex (9 parcels, $t=-8.6–3.6$, $p = 0.001–0.025$ FDR corrected) and left and right posterior cingulate cortex (7 parcels, $t=-5.9–3.3$, $p = 0.002–0.045$ FDR corrected). A full list of significant parcels are listed in Supplementary Table 1.

When the cortical parcellations were represented in the 3D gradient space, the activations appeared to congregate in approximately one third of the space. Specifically, when the task activations were discretized along the functional gradient in bins, a large number of activations occurred at the bottom third of Gradient 3, regions that are commonly implicated in attentional processing (Fig. 3B). This downsampling approach led to higher t-values in Gradient 3 (multiple-demand to paralimbic) than on the other gradient axes, as the regions specifically active in the task were grouped together and averaged along this gradient axis. However, there were also significant activations in the third quadrant of gradient 1 (bins 28–38).

The greatest magnitude of activations during the 2-back task (contrasted against 0-back) were observed in the dorsolateral prefrontal cortex (2 parcels, $t = 3.3–9.1$, $p = 0.001–0.022$ FDR corrected), frontal eye fields (6 parcels, $t = 3.0–6.9$, $p = 0.001–0.034$ FDR corrected), lateral prefrontal cortex (9 parcels, $t = 2.99–4.85$, $p = 0.003–0.033$), inferior parietal sulcus (8 parcels, $t = 3.1–3.99$, $p = 0.005–0.027$ FDR cor-

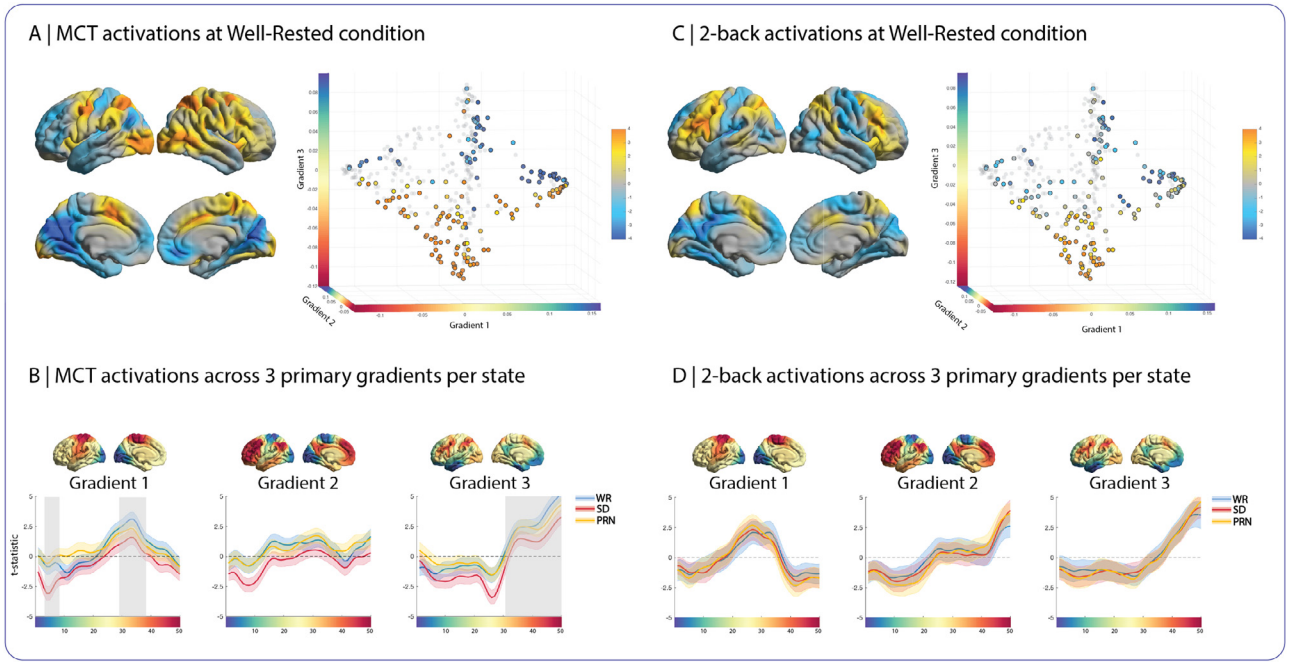

Fig. 3. Task evoked activations during tasks of vigilance and working memory. **A.** Task activations along the cortical surface and the 3D gradient space in the WR state during the Mackworth Clock Task (MCT). Each point in the scatterplot represents a parcel, and coloured (non-shaded) points represent significant activations after correction for comparisons across the cotex (FDR $p<0.05$). Each axis of the 3D space is colored to represent the direction of each gradient. **B.** Task activations in all parcels were averaged across 50 bins after being ordered along each gradient for each state (WR, SD, PRN). Lines represent mean activation per bin across subjects, and shading represents standard deviation. gray shading blocks indicate a statistically significant state-dependent change in activation (F-test, FDR corrected for multiple comparisons across gradient bins). Colours along each x-axis represent the direction of each gradient, as illustrated on the cortical surface representation above each graph. **C**. Task activations along the cortical surface and the 3D gradient space in the WR state during the 2-back vs 0-back task. Each point in the scatterplot represents a parcel, and coloured (non-shaded) points represent significant activations after correction for comparisons across the cotex (FDR $p<0.05$). Each axis of the 3D space is colored to represent the direction of each gradient. **D.** Task activations in all parcels were averaged across 50 bins after being ordered along each gradient for each state (WR, SD, PRN). Lines represent mean activation per bin across subjects, and shading represents standard deviation. Colours along each x-axis represent the direction of each gradient.

rected), and superior parietal lobule (8 parcels, $t = 2.7–4.87$, $p = 0.003–0.049$ FDR corrected; Fig. 3C). There were also significant deactivations within the left and right somatomotor cortex (17 parcels, $t = −5.3–2.7$, $p = 0.003–0.045$ FDR corrected), posterior cingulate cortex (6 parcels, $t= −5.2–2.8$, $p = 0.003–0.045$ FDR corrected), and superior extrastriate cortex (6 parcels, $t= −4.8–3.4$, $p = 0.003–0.019$). A full list of significant parcels is shown in Supplementary Table 2. Similar to the MCT, parcels with significant task activations appeared to congregrate in a third of the 3D gradient space, while deactivations were spread across the top half of the space. Again, when the task activations were discretized along the functional gradient in bins, the most substantial activations occurred at one end (multiple-demand) of gradient 3 (Fig. 3D). However, there were also activations present at one end (transmodal) of gradient 2, and a peak towards the center of gradient 1. Activations for the contrast 1-back vs 0-back are presented in Supplementary Fig. 1A and 1B).

During the ANT task, there were activations in the superior parietal lobe (SPL, Dorsal Attention Network), extrastriate cortex (Central Visual Network), left inferior parietal sulcus and insular cortex (small activation patterns, all uncorrected for multiple comparisons at $p<0.05$, Supplementary Fig. 1C). Additionally there were deactivations in the PCC (Default Mode Network), left auditory cortex, and extensive deactivations in the left somatomotor cortex (all uncorrected for multiple comparisons at $p<0.05$). Two parcels survived correction for multiple comparisons across all cortical parcels: left somatomotor cortex ($t = −4.78$, $p = 0.026$) and right SPL ($t = 5.33$, $p = 0.016$; Supplementary Table 3). Despite reduced power, the trends were similar for the ANT compared to the MCT and 2-back task when discretizing the task activations into 50 gradient bins (Supplementary Fig. 1D), with the greatest activations occuring at the end of gradient 3.

3.2. Changes in cortical activations following sleep deprivation and recovery nap

Changes in cortical activations during the MCT are shown in Supplementary Fig. 2A. Uncorrected for multiple comparisons, there were significant reductions in activity in parcellations belonging to the central visual, dorsal attention and tempoparietal networks after SD compared to WR (Supplementary Table 4, Cohen's $d_{average} = 0.64$). One parcel, located within the dorsal attention network, survived correction for multiple comparisons (across significantly active parcels at baseline). Following the PRN, there was an increase in activation in the same region. Investigating differences across the gradient bins however yielded a wider area of difference - the increased sensitivity arising due to clustering of regions into a reduced number of regions basd on their similar profile of functional connectivity (Fig. 3B). Specifically, there were significant reduced activations during the SD state compared to the WR state in gradient 1 in the middle (bins 30:36, $t= −3.4–2.9$) and increased deactivations toward the visual end (bins 5:7, $t = −3.0–3.2$). Additionally, there were significant reduced activations following SD compared to the WR state the end of gradient 3 (multiple-demand) that exhibited the greatest task-evoked activations in the WR state (20 bins, $t= −3.39–2.63$, $p<0.05$ FDR corrected). Following the PRN, activations recovered only in the regions at the visual end of gradient 1 (all $t = 3.4–3.9$). No other changes in bins were signficant between states.

For the 2-back task, there were slight reductions in very focal areas on the cortical surface, including the left supraparietal lobule, and left and right medial parietal lobe (Supplementary Table 5, Supplementary Fig. 2B, $d_{average} = 0.61$), however these did not survive multiple comparison correction. When discretized into bins along each gradient, we

found no significant state-dependent differences in activations during the 2-back task (Fig. 3D).

Changes in cortical activations during the ANT are shown in Supplementary Fig. 2C ($d_{average}$ = 0.69). No parcels survived multiple comparison correction between any of the states. When discretized into bins, there were no significant state-dependent differences in activation across the gradient bins for all three gradients.

3.3. Changes in functional gradients following sleep deprivation and recovery nap

There were no significant state-dependent changes in the range of gradient 1 ($F_{19,1}$ = 2.85, p = 0.071), gradient 2 ($F_{19,1}$ = 1.28, p = 0.289) or gradient 3 ($F_{19,1}$ = 1.79, p = 0.180; Fig. 4A). Between WR and SD states, the range of gradient 1 (0.23±0.03 vs 0.21±0.03; t= −1.83, p = 0.083, d = 0.52) and gradient 3 (0.18±0.02 vs 0.16±0.03; t= −1.85, p = 0.080, d = 0.55) trended towards a decrease, but not gradient 2 (0.17±0.02 vs 0.17±0.02; t= −0.17, p = 0.969, d = 0.04). There were no significant differences in the range of any gradient between the SD and PRN states. Furthermore, the distribution of parcels along each gradient did not significantly change across diferent states (Fig. 4B).

Parcels that were the furthest distance away from all others (i.e. exhibited the lowest centrality) in the 3D gradient space (Fig. 4C) also showed the greatest state-dependent shifts in centrality (r = 0.65, p < 0.001, $d_{average}$ = 1.03); Fig. 4D). This mostly incorporated parcels in the visual areas, but also included the posterior cingulate cortex (PCC). Specifically, the visual areas moved down gradient 1 (toward the somatomotor end) and gradient 2 (toward the transmodal end), while the parcels in the PCC moved down gradient 3 (toward the multiple-demand end; Fig. 4E). These parcels all shifted back in the opposite direction from the SD to the PRN state, indicating partial recovery of these changes.

Compared to the WR state, following SD there was a significant increased dispersion of the Visual B network (t = 3.56, p = 0.036 FDR corrected), but no other network. In addition, as whole communities, the two visual networks increased their mean centrality in the entire 3D gradient space, in the SD compared to the WR state, shifting towards all other networks (t = −3.3–4.1, p<0.05 FDR corrected). At the PRN state the centrality of these two networks did not significantly change. There were no other significant shifts in centrality of any other functional network. The pairwise distance between all parcels in the 3D gradient space demonstrated that parcels within the visual networks moved towards all other parcels following SD compared to the WR state (Fig. 5C). Notably, parcels within the somatomotor and dorsal attention B networks also moved away from all other parcels in the 3D gradient space.

To further investigate the correspondence between the functional gradients across vigilance states, we compared the three primary gradients between each state omitting alignment with Procrustes rotation. Spearman rank correlations between gradients from different states were on average 0.89 (range 0.82 - 0.98), demonstrating a high degree of similarity in these gradients across states.

3.4. The effect of global signal regression

Based on previous reports that the global signal fluctuation increases after SD, the global signal (GS) was compared across states. Consistent with this earlier work, we defined GS to be the mean time series obtained by averaging the preprocessed BOLD time courses across all cortical gray matter parcels, and the GS fluctuation as the temporal standard deviation of the GS (Orban et al., 2020; Wong et al., 2013). Indeed, the global signal fluctuation was significantly greater in the SD compared to the WR state (average standard deviation = 2.5 (SD) vs 1.9 (WR), t = 3.54, p = 0.002, d = 0.95). The global fluctuation did not significantly decrease following PRN (sd = 2.4, t= −0.82, p = 0.422, d = 0.12).

After performing GSR on the BOLD timeseries, we repeated all the analyses reported above. GSR had a significant impact on the changes observed in functional connectivity (Fig. 5A). Specifically, while a widespread increase in functional connectivity was observed between the WR and SD states when GSR was omitted, there was instead a mix of both increases and decreases in functional connectivity when GSR was applied, as expected by the positive and negative correlations usually observed after GSR. At the network level, there was an increase in functional connectivity between certain networks (such as the DMN and attentional networks), and a decrease in functional connectivity within certain networks (such as the DMN, ventral attention, and visual networks).

Performing GSR resulted in an overall reduction in the range of gradient 3 at the WR state (t= −2.9, p = 0.009; Fig. 5B). However it did not significantly alter the observed changes in the three gradients after sleep deprivation. Reductions in the range of the gradients followed the same trends as when GSR was omitted (Supplementary Fig. 3A). Regarding the shift in centrality of cortical parcels in the 3D gradient space, performing GSR resulted in the same observed shifts in centrality, however the movement of parcellations in the posterior cingulate cortex along Gradient 3 was more extensive (Supplementary Fig. 3C).

GSR reduced the largest changes in the pairwise distance in 3D gradient space between the WR and SD states (Fig. 5C). While parcels within the visual networks moved toward all other parcels, the magnitude of this distance was reduced following GSR. Similar trends were observed for parcels in the somatomotor networks moving away from all other parcels. Furthermore, GSR emphasised other specific changes, such as the DMN moving closer to the attention and fronto-parietal control networks.

3.5. Task performance before and after sleep deprivation and post recovery nap

Mean performance scores during each task are depicted in Fig. 1C and reported in Supplementary Table 6. As expected, across all tasks outcomes were significantly impaired following sleep deprivation, and improved following the recovery nap. In the MCT, mean reaction time increased from the WR to the SD state (q = 5.41, 95%CI = −43.6 to −8.8, p = 0.003, d = 0.48), and decreased from the SD to PRN state (q= −5.82, 95%CI = 11.2 to 47.3, p = 0.004, d = 0.57), but there were no differences between the WR and PRN states (q = 0.62, 95%CI = −14.5 to 20.5, p = 0.673; $F_{1,19}$ = 10.71, η^2 = 0.056; p<0.001, d = 0.05). Accuracy on the MCT also decreased from the WR to the SD state (q=−4.73, 95%CI = 2.8 to 20.9, p = 0.009, d = 0.60), and increased from the SD to PRN state (q = 4.59, 95%CI = −19.2 to −2.3, p = 0.011, d = 0.59), but there were no differences between the WR and PRN states (q = 0.63, 95%CI = −5.5 to 7.8, p = 0.606; $F_{1,19}$ = 8.45, η^2 = 0.078, p = 0.002, d = 0.06). In the ANT, there were mean reaction time differences between the WR and SD states (q = 5.66, 95%CI = −111.4 to −24.9, p = 0.002, d = 1.29), and between the SD and PRN states (q= −5.45, 95%CI = 18.9 to 91.9, p = 0.003, d = 0.78), but not between the WR and PRN states (q = 1.26, 95%CI = −49.3 to 23.8, p = 0.654; $F_{1,19}$ = 11.19, η^2 = 0.093, p<0.001, d = 0.15). Accuracy decreased from the WR to the SD state (q = 5.43, 95%CI = 7.1 to 34.6, p = 0.003, d = 0.71), and decreased from the SD to PRN state (q= −5.03, 95%CI = −25.4 to −4.2, p = 0.006, d = 0.56), but there were no differences between the WR and PRN states (q = 2.13, 95%CI = −4.1 to 16.2, p = 0.309; $F_{1,19}$ = 10.99, η^2 =0.204, p<0.001, d = 0.46). In the 2-back task, mean reaction time increased between the WR and SD states (q = 5.31, 95%CI = −366.1 to −70.6, p = 0.004, d = 1.06), and decreased between the SD and PRN states (q= −4.42, 95%CI = 27.5 to 267.0, p = 0.015, d = 0.61), but did not significantly change between the WR and PRN states (q = 2.78, 95%CI = −163.1 to 20.8, p = 0.148; $F_{1,19}$ = 10.76, η^2 = 0.161, p<0.001, d = 0.44). Accuracy decreased from the WR to the SD state (q = 5.02, 95%CI = 3.2 to 19.5, p = 0.005, d = 1.33), and decreased from the SD to PRN state (q= −4.73, 95%CI = −13.7 to −1.9, p = 0.009, d = 0.76), but there were no differences between the WR and PRN states (q = 2.88, 95%CI = −0.9 to 8.1, p = 0.13; $F_{1,19}$ = 10.77, η^2 =0.226, p = 0.001, d = 0.66).

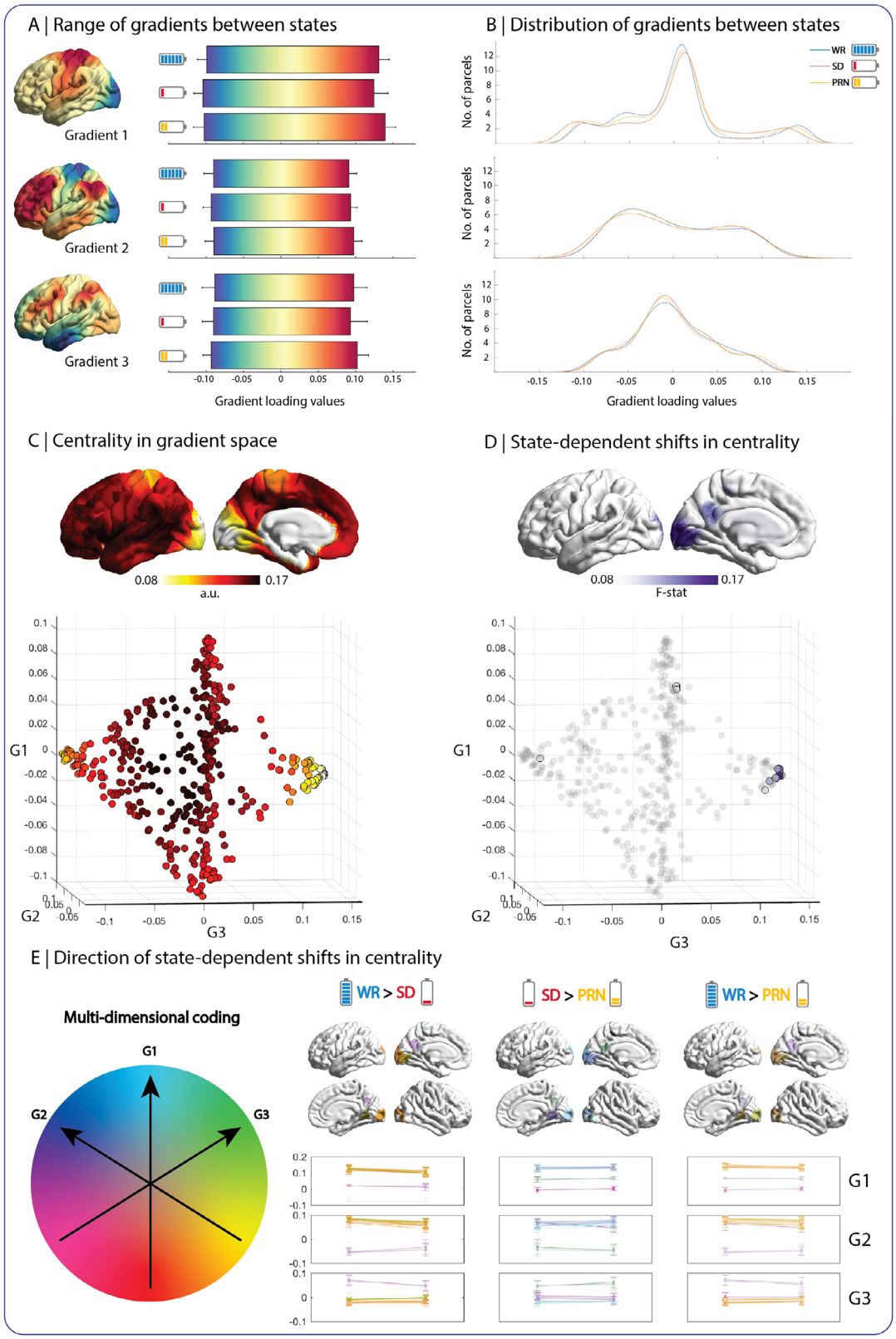

Fig. 4. Changes in functional gradients across the Well-Rested (WR), Sleep-Deprived (SD) and Post-Recovery Nap (PRN) states. **A**. The range of each gradient did not statistically change across states. **B**. The distribution of parcels within gradients did not significantly change across states **C**. In the WR state, the visual and somatomotor areas exhibited the lowest centrality in the 3D gradient space. **D**. Only parcels in the visual and the posterior cingulate cortex demonstrated state-dependent shifts in centrality (F = 1.2–15.9, p<0.05 FDR corrected). Coloured points in the scatterplot represent significantly thresholded parcels. **E**. *Left*: Multi-dimensional color-coding to represent along which gradient axes were the primary directions of each significant state-dependent shift in centrality in the 3D gradient space (from D). *Top*: The cortical parcels demonstrating state-dependent shifts in centrality are highlighted with the color indicating the direction of their primary shifts in the 3D space. *Bottom*: These parcels are displayed back on each gradient in each state to demonstrate the shifts of these parcels up and down each individual gradient.

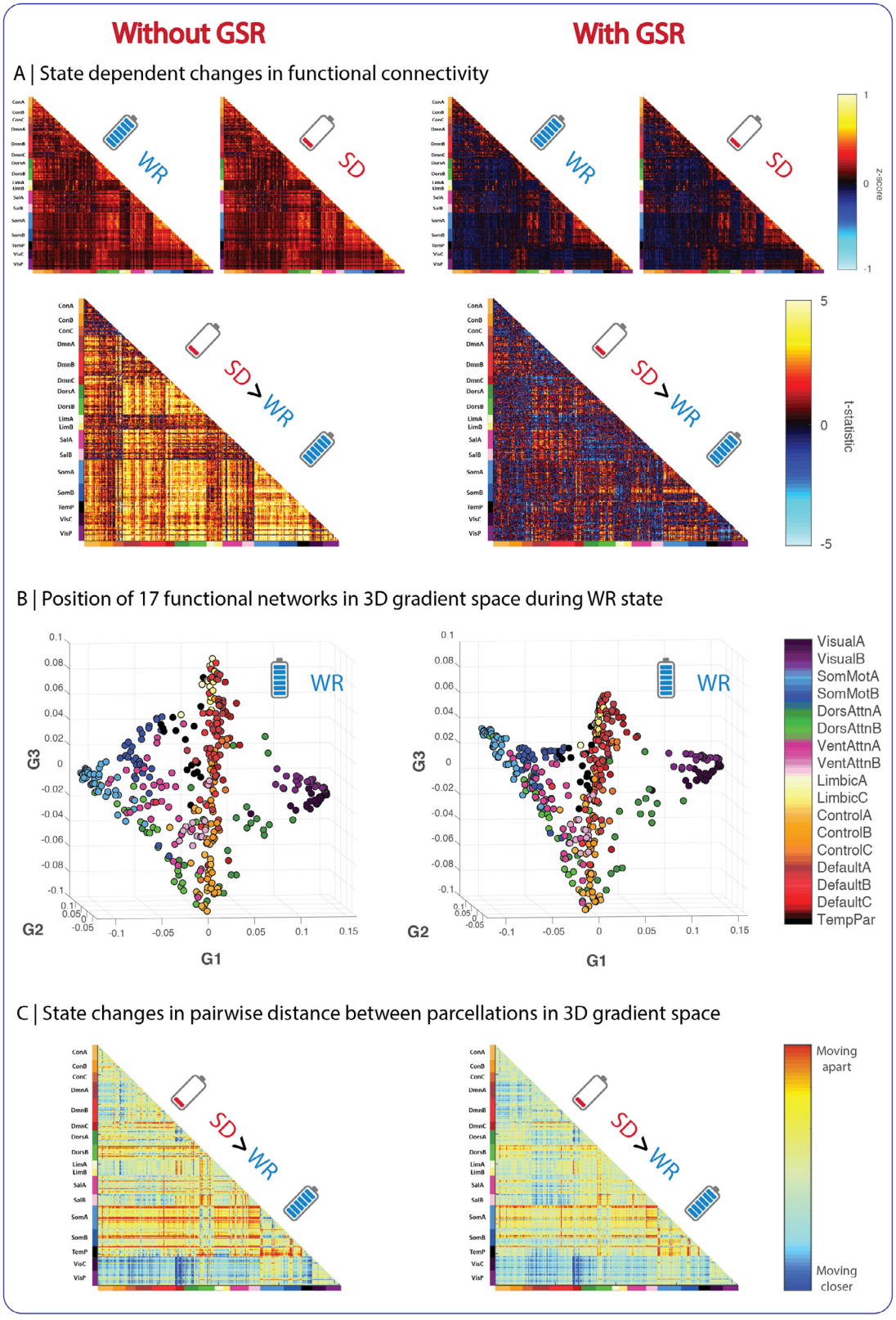

Fig. 5. The effect of global signal regression (GSR) on functional connectivity of the cortex and functional gradients. **A.** When GSR was not performed, there was a widespread increase in functional connectivity in the SD state when compared to the WR state, when considering standard connectome analysis. When GSR was performed, the difference between states was reduced, and mixed increases and decreases in connectivity between networks were observed. **B.** When represented in the 3D gradient space, 17 global functional networks clearly cluster in particular regions of the space, highlighting the organizing principle of the gradients. GSR reduced the range of Gradient 3 but otherwise the gradients in 3D space remained similar. **C.** State dependent changes the pairwise distance in 3D gradient space between the WR and SD states. GSR reduced the largest shifts in distance that were observed when it was not performed, and emphasised other specific changes, such as the DMN moving closer to the attention and fronto-parietal control networks.

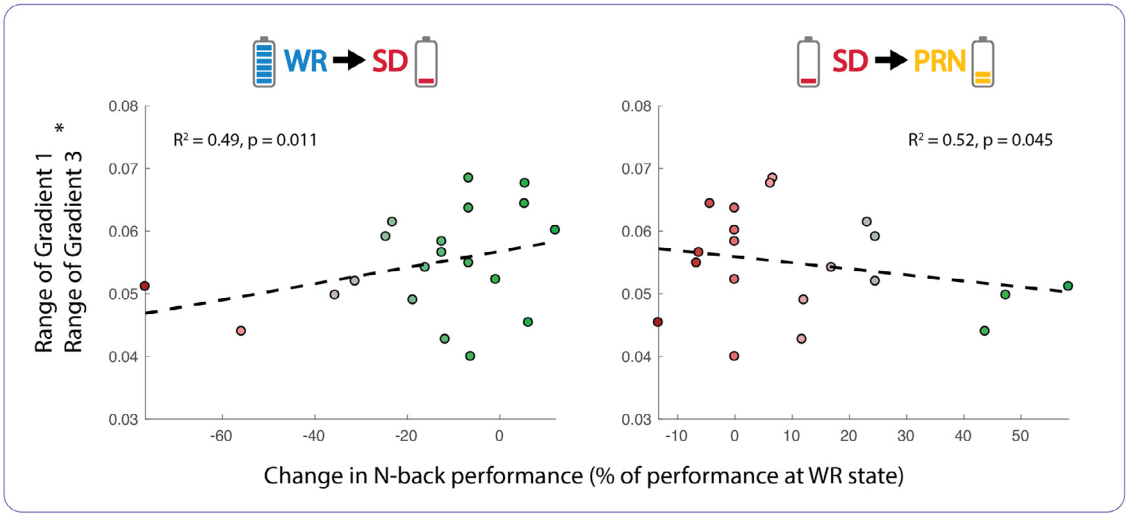

Fig. 6. The relationship between the interaction between ranges of functional gradients in the cortex at rested wakefulness (WR) and the change in performance on the 2-back task due to sleep deprivation (SD) and post a recovery nap (PRN). Each point represents a participant. Units on y-axis represent the sum of gradient ranges - these are arbitrary units but have been aligned across subjects for comparability using Procrustes rotation. R^2 values correspond to the regression model which included the individual ranges of both gradients and their interaction terms. Colors illustrate the change in 2-back performance to identify participants more resilient (green) from those more vulnerable (red) to SD (left scatter plot), and those who recovered more (green) from those who recovered less (red) after the nap (right scatter plot).

3.6. The relationship between functional gradients and behavior

The magnitude of task-evoked activations in any cortical parcel during the WR state were not significantly related to any reductions in performance on the MCT, ANT or 2-back task (for either reaction time or accuracy). The reduction in activations observed within the bins of gradient 1 or at the end of gradient 3 during the MCT in the SD state were not correlated with changes in either reaction time or accuracy on this task.

A stepwise linear regression model used to assess the relationship between gradient ranges and the decline in performance following SD, showed that the range of gradient 1 (Somatomotor-Visual) and gradient 3 (multiple-demand to paralimbic) in the WR state were together significant predictors of the decline in accuracy on the 2-back task ($F_{1,16} = 5.17$, $R^2 = 0.49$, $p = 0.011$) (Fig. 6). Similarly the range of these two gradients also predicted the extent of improvement in accuracy at the 2-back task following the PRN ($F_{1,16} = 3.08$, $R^2 = 0.52$, $p = 0.045$) (Fig. 6). There was no relationship between the range of gradients and changes in performance on the MCT, or performance related to the Alerting or Orienting stages of the ANT. The association with the Executive stage of the ANT was weak ($F_{1,18} = 4.39$, $R^2 = 0.20$, $p = 0.051$), with only the range of the third gradient as a variable in the model.

Multivariate PLS analysis identified two statistically significant latent variables (LVs) representative of shared covariance between gradient dispersion metrics (dispersion of networks within the 3D gradient space) and cognitive performance at the WR state. The first LV (permuted $P = 0.008$) accounted for 75% of the cross-block covariance. The strongest contributors to the first LV were the range of gradient 1, and the dispersion of the Ventral Attention B, Dorsal Attention B, and Default Mode C networks. However, there were no significant relationships between the dispersion of large-scale networks within the 3D gradient space and the change in performance on any of the tasks relating to SD. The first latent variable from the PLS analysis was the only variable that approached significance (permuted $P = 0.067$), despite accounting for 73% of the covariance between gradient dispersion metrics and cognitive function.

4. Discussion

By decomposing functional connectivity across the entire cortex into primary axes of differentiation, we were able to further probe the effects of sleep deprivation on cognitive and functional processes in the brain. The emerging approach of situating the activity of the cortex along gradients of differentiation was used under the assumption that it constitutes a basic structure of brain organization that constrain cognitive processes, and thus may be informative for exposing features of this organization that are related to brain states (Karapanagiotidis et al., 2019). This technique extends upon the idea of capitalizing on intrisinic coordinate systems - naturally occurring axes based on function rather than those in physical space - to study the organization of the human cortex. By using the normalized cosine angle between rows in the functional connectivity matrix, this approach is actually sensitive to the shape of the functional connectivity profiles rather than to the variations in amplitude. Such an approach makes it possible to compare the shapes of connectivity profiles, providing an analysis of the underlying structure of statistical dependencies among cortical regions.

Here, we leveraged three primary gradients relevant for hierarchical information processing in the brain, in line with what has been previously reported (Bethlehem et al., 2020; Karapanagiotidis et al., 2019; Margulies et al., 2016; Murphy et al., 2019). In particular, we found that the third gradient, extending from regions in frontoparietal and attention networks (multiple-demand) to paralimbic areas, was relevant for the cognitive processes involved in both vigilance and working memory tasks, which was validated by the task-evoked activations.

4.1. Cortical gradients represent cognitive processes

When cortical activations during attention and working memory tasks were averaged across bins of each gradient, clearly discernable sections of gradients exhibited significant elevated activity related to either task. This pattern of task activation assisted with conceptually defining the gradients within a cognitive framework. Relevant to both the attention and working memory tasks was activity at the end of the third gradient, which corresponded to fronto-parietal regions and is consistent with previous evidence that activity in these regions is linked with executive

control (multiple-demand) and goal-oriented cognition (Harding et al., 2015; Spreng et al., 2010). Specifically relevant to the 2-back task of working memory was activity at the very extreme end of the second gradient. These reflect transmodal regions previously shown to serve higher order functions such as the manipulation of incoming sensory information for integration with internal knowledge (Margulies et al., 2016; Murphy et al., 2019). While activations for the ANT were statistically weaker, this was likely due to the use of a trial-based design over a block-design for this task (Maus et al., 2010). Overall, these findings directly support the notion that functional gradients are relevant for activity patterns underlying ongoing cognitive processes.

We also found that averaging across bins of the functional gradients provided greater sensitivity in detecting state dependent changes in task-evoked cortical activations. On the MCT task in particular, while reduced activity was observed in key ROIs that have been specifically studied previously (Bell-McGinty et al., 2004; Chee and Tan, 2010; Chuah et al., 2006; Drummond et al., 2005; Lim et al., 2007; Tomasi et al., 2009), very few of the changes in activations survived corrections for multiple comparisons across the entire 400 cortical parcellations, indicating the limited magnitude of these changes in the context of whole cortical activity. However, when these activations were averaged across gradient bins, significant reductions following SD were observed in a consistent range of bins - given their functional similarity defined by this gradient. This highlights another potential benefit of using gradients for dimensionality reduction in task-based analysis of brain activity, especially when it is not feasible to recruit large cohorts (i.e. in certain clinical populations or using complex multi-modal imaging) to detect subtle, yet meaningful changes.

4.2. Functional gradients express minor state dependent changes following sleep deprivation

Despite observing a general widespread increase in functional connectivity following sleep deprivation, the functional gradients displayed a relatively high degree of stability (Fig. 4), i.e. the shape of the overall functional connectivity structure was preserved even if the overall amplitude was modulated. The visual system exhibited the greatest state dependent shifts, suggesting the functional connectivity profile of the visual regons became less independent following SD. This is likely due to its extreme position in the gradient space at rested wakefulness. The characteristic pattern of information processing in the visual system follows a very ordered hierarchy (Mishkin et al., 1983), tightly correspondant with microstructure (Rosenke et al., 2018) and gradients of gene expression (Gomez et al., 2019), and thus can be notably distinguished from the rest of the cortex. There was also a significant state-dependent shift in the centrality of the posterior cingulate cortex, particularly towards executive centres. The relatively strong connections between the PCC and the rest of the DMN are decreased during light sedation (i.e. a reduced level of waking consciousness; (Greicius et al., 2008), as well as disconnecting from anterior nodes of the DMN (i.e. ACC, MPFC) as sleep deepens (Horovitz et al., 2009). Furthermore, the PCC specifically displays significantly lower cerebral blood flow (Carhart-Harris et al., 2012) and higher desynchronisation (Muthukumaraswamy et al., 2013) during psychedelic states. In the context of these findings, the current results implicate the PCC as a region potentially susceptible to the quality of conscious states.

It was noticed that the range of gradient 1 (somatomotor-visual) and gradient 3 (multiple-demand to paralimbic) displayed a trend towards a decrease following sleep deprivation, even if this was not statistically significant. While reductions in these gradients following sleep deprivation would be consistent with an increase in global connectivity (i.e. reduced differentiation of function), the vulnerability of these axes to state-dependent changes needs to be confirmed in a larger sample before any conclusions could be made. More subtle differences in functional connectivity may have occurred that could not be observed with the power of the current sample, like as has been shown for network segregation (Yeo et al., 2015).. Nevertheless, these gradients are presumed to be a fundamental organizing principle of the brain, and here we provide evidence that they do not undergo major state dependent changes following sleep deprivation. The relative stability of the gradients across states is not surprising, if the view is held that these gradients encompass a general architecture of brain function. This is also supported by the ordered arrangement of well-defined cortical networks within the gradient space (Fig. 5B). While an increase in connectivity means regions become more similar in their function, if this happens globally in a relatively uniform manner, then the relationship of specific cortical parcels or networks to each other would become more uniform but should not rearrange.

We have therefore provided evidence that there are no large-scale changes in the functional organizing gradients of the cortex following sleep deprivation. This is an important aspect for consideration in future studies examining differences in functional gradients across clinical disorders, as changes, especially in the primary gradients, would be less dependent on state and therefore may be more reliable measures of underlying cortical architecture.

4.3. Gradients of cortical differentiation as predictors of vulnerability to sleep deprivation

A previous study reported that resilience to impaired vigilance following SD may be partially related to the range of segregation between certain cortical networks within some individuals (Yeo et al., 2015). We have extended this by showing that individual changes in working memory and executive attention are associated with the range of certain functional gradients, precisely gradients describing the differentation of somatomotor and visual regions, and multiple-demand to paralimbic regions. These findings suggest that the extent of differentiation across axes of cortical organization may be important traits for preserving cognitive processes following SD, when widespread cortical activity becomes more similar. While promising, these results are only preliminary given the current sample size and require further confirmation.

The dispersion of functional networks within the gradient space was significantly predictive of cognitive performance at the WR state. While cross-validation for out of sample prediction was not feasible given the sample size, this nevertheless suggests that these metrics of network segregation may be relevant for constraining cognition in the brain. However, the dispersion of functional networks in gradient space was not a significant predictor of declining performance following SD. The major difference between the range of gradients and the dispersion of functional communities within the multidimensional gradient space, is that the former represents differentiation of the entire cortex along a particular axis, while the latter reflects the clustering of separate functional systems in a hierarchical framework. Recent work has shown that dispersion of functional networks within a similar 3D gradient space is associated with age-related cognitive decline (Bethlehem et al., 2020). While aging is linked with considerable changes in brain structure, cognitive changes due to sleep deprivation are likely not, which may explain why they did not inform state-dependent cognitive changes in this sample of healthy younger adults.

Another possible explanation for this may be that reducing data from connectivity matrices to the primary axes of variance removes information that is instructive to accurately classify vulnerable individuals. It is plausible that gradients (particularly the primary axes) provide the scaffold for cognition to arise generally (Karapanagiotidis et al., 2019), and the variation among young, healthy individuals is not great enough to sufficiently detect (the notably variable) state dependent changes in cognition. It is plausible that additional functional gradients might be informative in this regard, however as yet the robustness and consistency of other functional gradients is yet unknown. Gradients have been extracted from data averaged over very large cohorts in young (Margulies et al., 2016) and older adults (Bethlehem et al., 2020), as well as newborns (Lariviere et al., 2020), showing some differences

in overall gradient organization, yet how consistent the gradients are across healthy individuals of the same age has not been extensively characterised. However, the fact that we have recreated very similar gradients in a smaller, independent sample suggests that these are inherent features of connectomes. Characteristics of gradients may be more suitable to explain cognitive processes in neurological or psychiatric conditions, where these deviations might be greater (and dependent on detectable variations in structure), rather than state dependent changes in healthy individuals. In support of this, an increasing body of studies in humans and non-human animals have suggested overlapping gradient configurations in the functional domain and those based on microstructural neuroimaging measures, including myelin sensitive MRI (Burt et al., 2018; Huntenburg et al., 2017; Paquola et al., 2019; Vos de Wael et al., 2018) and structural wiring features more generally (Paquola et al., 2020; Vazquez-Rodriguez et al., 2019) together with transcriptomic studies suggesting gene expression gradients that underpin macroscale functional hierarchies (Burt et al., 2018; Fulcher et al., 2019; Huntenburg et al., 2020).

The relative stability of functional gradients across the cortex across different arousal states offers important insight into the functional changes within the cortex following total sleep deprivation and the impact this has for cognition. Apart from dimensionality reduction, the gradient approach comments on the shape of functional connectivity profiles. While these profiles appear important for constraining cognitive processes generally, sleep deprivation does not seem to impair cognition through any alterations to the shape of these profiles. It does however appear to significantly impact the amplitude of connectivity in a widespread manner, although some edges between networks might be slightly more influenced (e.g. between visual networks and all other networks, DMN and attention networks). This is consistent with previous work, such that modularity of brain networks is decreased (Ben Simon et al., 2017), and subtle effects between similar networks are only observed following GSR (Yeo et al., 2015).

This notion of sleep deprivation affecting the amplitude and not the shape of functional connectivity profiles is supported by the widespread increase in functional connectivity, and the increased in the amplitude of the global signal fluctuation in the SD state. Here we replicated findings that fluctuations of the global signal of brain activity are increased following sleep deprivation (Yeo et al., 2015). Whilst relatively preserving the 3D gradient space at the WR state, performing GSR did have an effect on state-dependent changes in the gradients. It particularly emphasised different aspects in the state-dependent movement of cortical parcellations in the Euclidean gradient space (which can be alternatively viewed as regions becoming more or less similar in their profile of functional connectivity). The substantial shifts of the somatotomotor networks (away from other networks) and visual networks (towards other networks) were dampened by GSR. This is also consistent with previous findings that GSR has the strongest effect on somatomotor and visual connectivity, which has been proposed to be due to high signal fluctuations in these regions (Xu et al., 2018), and would likely be accentuated during tasks. Furthermore, GSR highlighted parcellations within the DMN undergoing state-dependent shifts towards the attentional networks following SD (Fig. 5C), consistent with previous findings that the DMN and attention networks become more connected following sleep deprivation (De Havas et al., 2012; Yeo et al., 2015), and may be related to the deficits in cognitive performance.

Despite evidence suggesting that global signal is likely related to neural activity and cognitive function (Li et al., 2019; Liu et al., 2017), these findings contribute to the discussion surrounding the use of GSR in fMRI analyses, and imply that it should be considered depending on the context and research question. Subtle or localized changes in functional connectivity might only become apparent once GSR is applied to the data (Li et al., 2019; Yeo et al., 2015), and this was corroborated in these findings as the association between gradients and changes in behavior were only evident once GSR was performed. Nevertheless changes in the global signal still appear to be an important aspect of sleep deprivation. Why this occurs and the relevance for sleepiness and arousal levels generally is yet to be determined.

4.4. Limitations

A few considerations must be acknowledged when interpreting these findings. Firstly, the sample size is relatively limited, although consistent with sample sizes previously reported for studies with complex methodologies during sleep (De Havas et al., 2012; Jegou et al., 2019). While it is possible that the lack of any significant state-dependent differences in the functional gradients could be related to statistical power, power analyses suggest that the current study was powered to observe moderate-large effects ($d > 0.6$), as demonstrated by the reported moderate to large effects in behavior, task activations, functional connectivity and global signal fluctuations. We thus still conclude that changes to the characteristics of functional gradients are minimal and less sensitive to sleep deprivation than the other reported measures. This study was designed to test multiple aspects of cognitive function deficits attributed to sleep deprivation, however the use of multiple tasks required a trade-off of a shorter task duration per task, which reduced the power of the task activation detection and could account for why the activations did not clear multiple comparison testing. The improvements in performance following the recovery nap could also be attributed to a practice effect, as repeated testing was not conducted on the WR visit. Counterbalancing the order of task presentation could have overcome limitations affecting fatigue on the tasks that were always presented last. However, given the small sample size, true randomization would not have been achievable with enough power and confidence. Furthermore, the functional connectivity was estimated from sequences acquired during performance of these cognitive tasks, and not resting state. Although the task-evoked responses were regressed from the BOLD timeseries, and connectivity estimates were highly correlated to those in the resting state of the WR condition, this was not equal to a resting state sequence. Therefore, this may explain some differences between the gradients reported in this study and those previously reported in studies using resting state sequences (Bethlehem et al., 2020; Hong et al., 2019; Margulies et al., 2016). In particular, the variance explained by each functional gradient differs amongst individuals (Bethlehem et al., 2020) and further research is necessary to assess the stability of functional gradients across individuals and datasets.

5. Conclusions

This study harnessed an emerging technique to explore the state-dependent brain activity changes following sleep deprivation and a recovery nap, and to further identify markers that may predict interindividual vulnerability to impaired cognitive performance. These findings contribute to a growing body of research indicating that cortical gradients of functional differentiation constitute low-dimensional organizing principles within the cerebral cortex that are relevant for the emergence of cognitive processes, demonstrated here by effectively representing brain activation patterns during tasks of attention and working memory. However, we show that these gradients do not exhibit major state dependent changes following sleep deprivation. This suggests that they may be trait-like characteristics of cortical organization, potentially related to properties of brain structure, however further research into the stability of gradients within individuals over time is needed in larger samples. Consistent with previous findings, we have shown that sleep deprivation results in a widespread increase in cortico-cortico functional connectivity and the fluctuation of the global signal, which might conceal subtle inter-individual differences that are predictive of state-dependent changes in cognition. Particularly, the range and extent of certain functional gradients within individuals might be important for constraining state-dependent changes in cognitive performance, but these perhaps need to be used in combination with other physiological measures to

determine a more comprehensive model of the effects of sleep deprivation on brain function.

Credit authorship contribution statement

Nathan Cross: Conceptualization, Methodology, Software, Formal analysis, Investigation, Data curation, Writing - original draft, Visualization, Project administration. **Casey Paquola:** Conceptualization, Methodology, Validation, Software, Writing - review & editing, Visualization. **Florence B. Pomares:** Investigation, Data curation, Writing - review & editing. **Aurore A. Perrault:** Writing - review & editing, Visualization. **Aude Jegou:** Investigation. **Alex Nguyen:** Investigation, Data curation. **Umit Aydin:** Investigation, Writing - review & editing. **Boris C. Bernhardt:** Methodology, Validation, Writing - review & editing. **Christophe Grova:** Conceptualization, Resources, Writing - review & editing, Supervision, Project administration, Funding acquisition. **Thien Thanh Dang-Vu:** Conceptualization, Resources, Writing - review & editing, Supervision, Project administration, Funding acquisition.

Acknowledgments

This research was supported by the Natural Sciences and Engineering Research Council of Canada (TDV) and the Canada Foundation for Innovation (TDV). The MRI compatible high-density EEG device (Philips Neuro) and data acquisition were made possible through an internal grant from PERFORM center and the Faculty of Arts ans Science of Concordia University (CG). TDV is also supported by the Canadian Institutes of Health Research (MOP 142191, PJT 153115, PJT 156125 and PJT 166167), the Fonds de Recherche du Québec – Santé and Concordia University. CG is supported Natural Sciences and Engineering Research Council of Canada Discovery grants as well as the Canadian Institutes of Health Research (PJT-159948 and MOP-133619) and the Fonds de Recherche du Québec, Nature et Technology (research team grant). BCB acknowledges research support from the National Science and Engineering Research Council of Canada (NSERC Discovery-1304413), the Canadian Institutes of Health Research (CIHR FDN-154298), Azieli Center for Autism Research, SickKids Foundation (NI17–039), and the Tier-2 Canada Research Chairs program.

Supplementary materials

Supplementary material associated with this article can be found, in the online version, at doi:10.1016/j.neuroimage.2020.117547.

References

Ayalon, R.D., Friedman, F., 2008. The effect of sleep deprivation on fine motor coordination in obstetrics and gynecology residents. Am. J. Obstet. Gynecol. 199, 576.e571–576.e575.

Bell-McGinty, S., Habeck, C., Hilton, H.J., Rakitin, B., Scarmeas, N., Zarahn, E., Flynn, J., DeLaPaz, R., Basner, R., Stern, Y., 2004. Identification and differential vulnerability of a neural network in sleep deprivation. Cereb. Cortex 14, 496–502.

Ben Simon, E., Maron-Katz, A., Lahav, N., Shamir, R., Hendler, T., 2017. Tired and misconnected: a breakdown of brain modularity following sleep deprivation. Hum. Brain Mapp. 38, 3300–3314.

Benjamini, Y., Hochberg, Y., 1995. Controlling the false discovery rate: a practical and powerful approach to multiple testing. J. R. Stat. Soc. Ser. B (Methodol.). 57 (1), 289–300.

Bethlehem, R.A.I., Paquola, C., Seidlitz, J., Ronan, L., Bernhardt, B., Consortium, C.C., Tsvetanov, K.A., 2020. Dispersion of functional gradients across the lifespan. Neuroimage 222, 117299. doi:10.1016/j.neuroimage.2020.117299, Epub ahead of print.

Blatter, K., Opwis, K., Münch, M., Wirz-Justice, A., Cajochen, C., 2005. Sleep loss-related decrements in planning performance in healthy elderly depend on task difficulty. J. Sleep Res. 14, 409–417.

Burt, J.B., Demirtas, M., Eckner, W.J., Navejar, N.M., Ji, J.L., Martin, W.J., Bernacchia, A., Anticevic, A., Murray, J.D., 2018. Hierarchy of transcriptomic specialization across human cortex captured by structural neuroimaging topography. Nat. Neurosci. 21 (9), 1251–1259.

Carhart-Harris, R.L., Erritzoe, D., Williams, T., Stone, J.M., Reed, L.J., Colasanti, A., Tyacke, R.J., Leech, R., Malizia, A.L., Murphy, K., Hobden, P., Evans, J., Feilding, A., Wise, R.G., Nutt, D.J., 2012. Neural correlates of the psychedelic state as determined by fMRI studies with psilocybin. Proc. Natl. Acad. Sci. U. S.A. 109 (6), 2138–2143.

Chee, M.W.L., Chuah, L.Y.M., Venkatraman, V., Chan, W.Y., Philip, P., Dinges, D.F., 2006. Functional imaging of working memory following normal sleep and after 24 and 35h of sleep deprivation: correlations of fronto-parietal activation with performance. Neuroimage 31, 419–428.

Chee, M.W.L., Tan, J.C., 2010. Lapsing when sleep deprived: neural activation characteristics of resistant and vulnerable individuals. Neuroimage 51, 835–843.

Choo, W.-.C., Lee, W.-.W., Venkatraman, V., Sheu, F.-.S., Chee, M.W.L., 2005. Dissociation of cortical regions modulated by both working memory load and sleep deprivation and by sleep deprivation alone. Neuroimage 25, 579–587.

Chuah, Y.M.L., Venkatraman, V., Dinges, D.F., Chee, M.W.L., 2006. The neural basis of interindividual variability in inhibitory efficiency after sleep deprivation. J. Neurosci. 26, 7156–7162.

Ciric, R., Wolf, D.H., Power, J.D., Roalf, D.R., Baum, G.L., Ruparel, K., Shinohara, R.T., Elliott, M.A., Eickhoff, S.B., Davatzikos, C., Gur, R.C., Gur, R.E., Bassett, D.S., Satterthwaite, T.D., 2017. Benchmarking of participant-level confound regression strategies for the control of motion artifact in studies of functional connectivity. Neuroimage 154, 174–187.

Cox, R.W., 1996. AFNI: software for analysis and visualization of functional magnetic resonance neuroimages. Comput. Biomed. Res. 29 (3), 162–173.

De Havas, J.A., Parimal, S., Soon, C.S., Chee, M.W.L., 2012. Sleep deprivation reduces default mode network connectivity and anti-correlation during rest and task performance. Neuroimage 59, 1745–1751.

Dennis, L.E., Wohl, R.J., Selame, L.A., Goel, N., 2017. Healthy adults display long-term trait-like neurobehavioral resilience and vulnerability to sleep loss. Sci. Rep. 7, 18–21.

Doran, S.M., Van Dongen, H.P., Dinges, D.F., 2001. Sustained attention performance during sleep deprivation: evidence of state instability. Arch. Ital. Biol. 139 (3), 253–267.

Drummond, S.P., Brown, G.G., Salamat, J.S., Gillin, J.C., 2004. Increasing task difficulty facilitates the cerebral compensatory response to total sleep deprivation. Sleep 27 (3), 445–451.

Drummond, S.P.A., Bischoff-grethe, A., Dinges, D.F., Ayalon, L., Mednick, S.C., Meloy, M.J., 2005. The neural basis of the psychomotor vigilance task. Sleep.

Drummond, S.P.A., Brown, G.G., Gillin, J.C., Stricker, J.L., Wong, E.C., Buxton, R.B., 2000. Altered brain response to verbal learning following sleep deprivation. Nature 403, 655–657.

Eckart, C., Young, G., 1936. The approximation of one matrix by another of lower rank. Psychometrika 1 (3), 211–218.

Elliott, M.L., Knodt, A.R., Cooke, M., Kim, M.J., Melzer, T.R., Keenan, R., Ireland, D., Ramrakha, S., Poulton, R., Caspi, A., Moffitt, T.E., Hariri, A.R., 2019. General functional connectivity: shared features of resting-state and task fMRI drive reliable and heritable individual differences in functional brain networks. Neuroimage 189, 516–532.

Esteban, O., Markiewicz, C.J., Blair, R.W., Moodie, C.A., Isik, A.I., Erramuzpe, A., Kent, J.D., Goncalves, M., DuPre, E., Snyder, M., Oya, H., Ghosh, S.S., Wright, J., Durnez, J., Poldrack, R.A., Gorgolewski, K.J., 2019. fMRIPrep: a robust preprocessing pipeline for functional MRI. Nat. Methods 16 (1), 111–116.

Esteban, O., C.J. Markiewicz, H. Johnson, E. Ziegler, A. Manhes-Savio, D. Jarecka, C. Burns, D.G. Ellis, C. Hamalainen, M.P. Notter, B. Yvernault, T. Salo, M. Waskom, M. Goncalves, K. Jordan, J. Wong, B.E. Dewey, C. Madison, E. Benderoff, D. Clark, F. Loney, D. Clark, A. Keshavan, M. Joseph, D.M. Nielson, M. Dayan, M. Modat, A. Gramfort, S. Bougacha, B. Pinsard, S. Berleant, H. Christian and A.A. Rokem. nipy/nipype: 1.4.2. 2020.

Fan, J., McCandliss, B.D., Fossella, J., Flombaum, J.I., Posner, M.I., 2005. The activation of attentional networks. Neuroimage 26 (2), 471–479.

Fan, J., McCandliss, B.D., Sommer, T., Raz, A., Posner, M.I., 2002. Testing the efficiency and independence of attentional networks. J. Cognit. Neurosci. 14 (3), 340–347.

Forest, G., Godbout, R., 2000. Effects of sleep deprivation on performance and EEG spectral analysis in young adults. Brain Cognit. 43 (1–3), 195–200.

Fulcher, B.D., Murray, J.D., Zerbi, V., Wang, X.J., 2019. Multimodal gradients across mouse cortex. Proc. Natl. Acad. Sci. U.S.A. 116 (10), 4689–4695.

Gevers, W., Deliens, G., Hoffmann, S., Notebaert, W., Peigneux, P., 2015. Sleep deprivation selectively disrupts top-down adaptation to cognitive conflict in the Stroop test. J. Sleep Res. 24, 666–672.

Gomez, J., Zhen, Z., Weiner, K.S., 2019. Human visual cortex is organized along two genetically opposed hierarchical gradients with unique developmental and evolutionary origins. PLoS Biol. 17 (7), e3000362.

Gorgolewski, K., Burns, C.D., Madison, C., Clark, D., Halchenko, Y.O., Waskom, M.L., Ghosh, S.S., 2011. Nipype: a flexible, lightweight and extensible neuroimaging data processing framework in python. Front. Neuroinform. 5, 13.

Greicius, M.D., Kiviniemi, V., Tervonen, O., Vainionpaa, V., Alahuhta, S., Reiss, A.L., Menon, V., 2008. Persistent default-mode network connectivity during light sedation. Hum. Brain Mapp. 29 (7), 839–847.

Greve, D.N., Fischl, B., 2009. Accurate and robust brain image alignment using boundary-based registration. Neuroimage 48 (1), 63–72.

Haak, K.V., Marquand, A.F., Beckmann, C.F., 2018. Connectopic mapping with resting-state fMRI. Neuroimage 170, 83–94.

Harding, I.H., Yucel, M., Harrison, B.J., Pantelis, C., Breakspear, M., 2015. Effective connectivity within the frontoparietal control network differentiates cognitive control and working memory. Neuroimage 106, 144–153.

Hong, S.-.J., Vos de Wael, R., Bethlehem, R.A.I., Lariviere, S., Paquola, C., Valk, S.L., Milham, M.P., Di Martino, A., Margulies, D.S., Smallwood, J., Bernhardt, B.C., 2019. Atypical functional connectome hierarchy in autism. Nat. Commun. 10 (1), 1022.

Horovitz, S.G., Braun, A.R., Carr, W.S., Picchioni, D., Balkin, T.J., Fukunaga, M., Duyn, J.H., 2009. Decoupling of the brain's default mode network during deep sleep. Proc. Natl. Acad. Sci. U.S.A. 106 (27), 11376–11381.

Huntenburg, J.M., Bazin, P.-.L., Margulies, D.S., 2018. Large-scale gradients in human cortical organization. Trends Cogn. Sci. (Regul. Ed.) 22 (1), 21–31.

Huntenburg, J.M., Bazin, P.L., Goulas, A., Tardif, C.L., Villringer, A., Margulies, D.S., 2017.

A systematic relationship between functional connectivity and intracortical myelin in the human cerebral cortex. Cereb. Cortex 27 (2), 981–997.
Huntenburg, J.M., Yeow, L.Y., Mandino, F., Grandjean, J., 2020. Gradients of functional connectivity in the mouse cortex reflect neocortical evolution. bioRxiv 2020.2003.2004.976860.
Jegou, A., Schabus, M., Gosseries, O., Dahmen, B., Albouy, G., Desseilles, M., Sterpenich, V., Phillips, C., Maquet, P., Grova, C., Dang-Vu, T.T., 2019. Cortical reactivations during sleep spindles following declarative learning. Neuroimage 195, 104–112.
Jenkinson, M., Bannister, P., Brady, M., Smith, S., 2002. Improved optimization for the robust and accurate linear registration and motion correction of brain images. Neuroimage 17 (2), 825–841.
Karakorpi, M., Alhola, P., Urrila, A.S., Kylmälä, M., Portin, R., Kalleinen, N., Polo-Kantola, P., 2006. Hormone treatment gives no benefit against cognitive changes caused by acute sleep deprivation in postmenopausal women. Neuropsychopharmacol. Off. Publ. Am. Coll. Neuropsychopharmacol. 31, 2079–2088.
Karapanagiotidis, T., Vidaurre, D., Quinn, A.J., Vatansever, D., Poerio, G.L., Turnbull, A., Leech, R., Bernhardt, B., Jefferies, E., Margulies, D.S., Nichols, T.E., Woolrich, M.W., Smallwood, J., 2019. Emergence of neural dynamics within a co-ordinate space of large-scale neural hierarchies. bioRxiv, 885772 2019.2012.2021.
Kendall, A.P., Kautz, M.A., Russo, M.B., Killgore, W.D., 2006. Effects of sleep deprivation on lateral visual attention. Int. J. Neurosci. 116 (10), 1125–1138.
Killgore, W.D., Balkin, T.J., Wesensten, N.J., 2006. Impaired decision making following 49h of sleep deprivation. J. Sleep Res. 15 (1), 7–13.
Kirchner, W.K., 1958. Age differences in short-term retention of rapidly changing information. J. Exp. Psychol. 55 (4), 352–358.
Kirschner, M., Shafiei, G., Markello, R., Makowski, C., Talpalaru, A., Hodzic-Santor, B., Devenyi, G., Paquola, C., Bernhardt, B., Lepage, M., Chakravarty, M., Dagher, A., Misic, B., 2020. Latent clinical-anatomical dimensions of schizophrenia. medRxiv 2020.2003.2025.20040592.
Krishnan, A., Williams, L.J., McIntosh, A.R., Abdi, H., 2011. Partial least squares (PLS) methods for neuroimaging: a tutorial and review. Neuroimage 56 (2), 455–475.
Lafon, S., Keller, Y., Coifman, R.R., 2006. Data fusion and multicue data matching by diffusion maps. IEEE Trans. Pattern Anal. Mach. Intell. 28 (11), 1784–1797.
Langs, G., Golland, P., Ghosh, S.S., 2015. Predicting activation across individuals with resting-state functional connectivity based multi-atlas label fusion. Med. Image Comput. Comput. Assist. Interv. 9350, 313–320 MICCAI ... International Conference on Medical Image Computing and Computer-Assisted Intervention.
Lariviere, S., Vos de Wael, R., Hong, S.J., Paquola, C., Tavakol, S., Lowe, A.J., Schrader, D.V., Bernhardt, B.C., 2020. Multiscale structure-function gradients in the neonatal connectome. Cereb. Cortex 30 (1), 47–58.
Li, J., Bolt, T., Bzdok, D., Nomi, J.S., Yeo, B.T.T., Spreng, R.N., Uddin, L.Q., 2019a. Topography and behavioral relevance of the global signal in the human brain. Sci. Rep. 9 (1), 14286.
Li, J., Kong, R., Liegeois, R., Orban, C., Tan, Y., Sun, N., Holmes, A.J., Sabuncu, M.R., Ge, T., Yeo, B.T.T., 2019b. Global signal regression strengthens association between resting-state functional connectivity and behavior. Neuroimage 196, 126–141.
Lichstein, K.L., Riedel, B.W., Richman, S.L., 2000. The Mackworth clock test: a computerized version. J. Psychol. 134 (2), 153–161.
Lim, J., Choo, W.C., Chee, M.W.L., 2007. Reproducibility of changes in behaviour and fMRI activation associated with sleep deprivation in a working memory task. Sleep 30, 61–70.
Linde, L., Edland, A., Bergström, M., 1999. Auditory attention and multiattribute decision-making during a 33h sleep-deprivation period: mean performance and between–subject dispersions. Ergonomics 42, 696–713.
Liu, T.T., Nalci, A., Falahpour, M., 2017. The global signal in fMRI: nuisance or Information? Neuroimage 150, 213–229.
Loh, S., Lamond, N., Dorrian, J., Roach, G., Dawson, D., 2004. The validity of psychomotor vigilance tasks of less than 10-minute duration. Behav. Res. Methods Instrum. Comput. 36 (2), 339–346.
Margulies, D.S., Ghosh, S.S., Goulas, A., Falkiewicz, M., Huntenburg, J.M., Langs, G., Bezgin, G., Eickhoff, S.B., Castellanos, F.X., Petrides, M., Jefferies, E., Smallwood, J., 2016. Situating the default-mode network along a principal gradient of macroscale cortical organization. Proc. Natl. Acad. Sci. U.S.A. 113, 12574–12579.
Maus, B., van Breukelen, G.J.P., Goebel, R., Berger, M.P.F., 2010. Optimization of blocked designs in fMRI studies. Psychometrika 75 (2), 373–390.
McIntosh, A.R., Lobaugh, N.J., 2004. Partial least squares analysis of neuroimaging data: applications and advances. Neuroimage 23 (Suppl 1), S250–S263.
McIntosh, A.R., Misic, B., 2013. Multivariate statistical analyses for neuroimaging data. Annu. Rev. Psychol. 64, 499–525.
Mesulam, M, 1994. Neurocognitive networks and selectively distributed processing. Rev. Neurol. (Paris) 150 (8–9), 564–569.
Mesulam, M.M, 1998. From sensation to cognition. Brain 121 (Pt 6), 1013–1052.
Millisecond Software LLC. Seattle USA.
Mishkin, M., Ungerleider, L.G., Macko, K.A., 1983. Object vision and spatial vision: two cortical pathways. Trends Neurosci. 6, 414–417.
Mišić, B., Betzel, R.F., de Reus, M.A., van den Heuvel, M.P., Berman, M.G., McIntosh, A.R., Sporns, O., 2016. Network-level structure-function relationships in human neocortex. Cereb. Cortex 26 (7), 3285–3296.
Murphy, C., Jefferies, E., Rueschemeyer, S.A., Sormaz, M., Wang, H.T., Margulies, D.S., Smallwood, J., 2018. Distant from input: evidence of regions within the default mode network supporting perceptually-decoupled and conceptually-guided cognition. Neuroimage 171, 393–401.
Murphy, C., Wang, H.T., Konu, D., Lowndes, R., Margulies, D.S., Jefferies, E., Smallwood, J., 2019. Modes of operation: a topographic neural gradient supporting stimulus dependent and independent cognition. Neuroimage 186, 487–496.
Muthukumaraswamy, S.D., Carhart-Harris, R.L., Moran, R.J., Brookes, M.J., Williams, T.M., Errtizoe, D., Sessa, B., Papadopoulos, A., Bolstridge, M., Singh, K.D., Feilding, A., Friston, K.J., Nutt, D.J., 2013. Broadband cortical desynchronization underlies the human psychedelic state. J. Neurosci. 33 (38), 15171–15183.
Muto, V., Jaspar, M., Meyer, C., Kusse, C., Chellappa, S.L., Degueldre, C., Balteau, E., Shaffii-Le Bourdiec, A., Luxen, A., Middleton, B., Archer, S.N., Phillips, C., Collette, F., Vandewalle, G., Dijk, D.J., Maquet, P., 2016. Local modulation of human brain responses by circadian rhythmicity and sleep debt. Science 353 (6300), 687–690.
Orban, C., Kong, R., Li, J., Chee, M.W.L., Yeo, B.T.T., 2020. Time of day is associated with paradoxical reductions in global signal fluctuation and functional connectivity. PLoS Biol. 18 (2), e3000602.
Paquola, C., Seidlitz, J., Benkarim, O., Royer, J., Klimes, P., Bethlehem, R.A.I., Lariviere, S., Vos de Wael, R., Hall, J.A., Frauscher, B., Smallwood, J., Bernhardt, B.C., 2020. The cortical wiring scheme of hierarchical information processing. bioRxiv 2020.2001.2008.899583.
Paquola, C., Vos De Wael, R., Wagstyl, K., Bethlehem, R.A.I., Hong, S.J., Seidlitz, J., Bullmore, E.T., Evans, A.C., Misic, B., Margulies, D.S., Smallwood, J., Bernhardt, B.C., 2019. Microstructural and functional gradients are increasingly dissociated in transmodal cortices. PLoS Biol. 17 (5), e3000284.
Rosenke, M., Weiner, K.S., Barnett, M.A., Zilles, K., Amunts, K., Goebel, R., Grill-Spector, K., 2018. A cross-validated cytoarchitectonic atlas of the human ventral visual stream. Neuroimage 170, 257–270.
Rupp, T.L., Wesensten, N.J., Balkin, T.J., 2012. Trait-like vulnerability to total and partial sleep loss. Sleep 35, 1163–1172.
Schaefer, A., Kong, R., Gordon, E.M., Laumann, T.O., Zuo, X.N., Holmes, A.J., Eickhoff, S.B., Yeo, B.T.T., 2018. Local-global parcellation of the human cerebral cortex from intrinsic functional connectivity MRI. Cereb. Cortex 28 (9), 3095–3114.
Shine, J.M., Breakspear, M., Bell, P.T., Ehgoetz Martens, K.A., Shine, R., Koyejo, O., Sporns, O., Poldrack, R.A., 2019. Human cognition involves the dynamic integration of neural activity and neuromodulatory systems. Nat. Neurosci. 22 (2), 289–296.
Spreng, R.N., Stevens, W.D., Chamberlain, J.P., Gilmore, A.W., Schacter, D.L., 2010. Default network activity, coupled with the frontoparietal control network, supports goal-directed cognition. Neuroimage 53 (1), 303–317.
Sweet, L.H., 2011. N-back paradigm. In: Kreutzer, J.S., DeLuca, J., Caplan, B. (Eds.), Encyclopedia of Clinical Neuropsychology. Springer, New York, NYNew York, pp. 1718–1719.
Tomasi, D., Wang, R.L., Telang, F., Boronikolas, V., Jayne, M.C., Wang, G.J., Fowler, J.S., Volkow, N.D., 2009. Impairment of attentional networks after 1 night of sleep deprivation. Cereb. Cortex 19, 233–240.
Van Dongen, H.P.A., Maislin, G., Mullington, J.M., Dinges, D.F., 2003. The cumulative cost of additional wakefulness. Sleep (Rochester) 26, 117–126.
Vazquez-Rodriguez, B., Suarez, L.E., Markello, R.D., Shafiei, G., Paquola, C., Hagmann, P., van den Heuvel, M.P., Bernhardt, B.C., Spreng, R.N., Misic, B., 2019. Gradients of structure-function tethering across neocortex. Proc. Natl. Acad. Sci. U. S. A. 116 (42), 21219–21227.
Vos de Wael, R., Benkarim, O., Paquola, C., Lariviere, S., Royer, J., Tavakol, S., Xu, T., Hong, S.J., Langs, G., Valk, S., Misic, B., Milham, M., Margulies, D., Smallwood, J., Bernhardt, B.C., 2020. BrainSpace: a toolbox for the analysis of macroscale gradients in neuroimaging and connectomics datasets. Commun. Biol. 3 (1), 103.
Vos de Wael, R., Lariviere, S., Caldairou, B., Hong, S.J., Margulies, D.S., Jefferies, E., Bernasconi, A., Smallwood, J., Bernasconi, N., Bernhardt, B.C., 2018. Anatomical and microstructural determinants of hippocampal subfield functional connectome embedding. Proc. Natl. Acad. Sci. U. S. A. 115 (40), 10154–10159.
Wang, C., Mahadevan, S., 2008. Manifold alignment using procrustes analysis. In: Proceedings of the ICML '08, pp. 1120–1127.
Wang, C., Ong, J.L., Patanaik, A., Zhou, J., Chee, M.W., 2016. Spontaneous eyelid closures link vigilance fluctuation with fMRI dynamic connectivity states. Proc. Natl. Acad. Sci. U. S. A. 113 (34), 9653–9658.
Wong, C.W., Olafsson, V., Tal, O., Liu, T.T., 2013. The amplitude of the resting-state fMRI global signal is related to EEG vigilance measures. Neuroimage 83, 983–990.
Xu, H., Su, J., Qin, J., Li, M., Zeng, L.L., Hu, D., Shen, H., 2018. Impact of global signal regression on characterizing dynamic functional connectivity and brain states. Neuroimage 173, 127–145.
Yeo, B.T., Krienen, F.M., Sepulcre, J., Sabuncu, M.R., Lashkari, D., Hollinshead, M., Roffman, J.L., Smoller, J.W., Zollei, L., Polimeni, J.R., Fischl, B., Liu, H., Buckner, R.L., 2011. The organization of the human cerebral cortex estimated by intrinsic functional connectivity. J. Neurophysiol. 106 (3), 1125–1165.
Yeo, B.T.T., Tandi, J., Chee, M.W.L., 2015. Functional connectivity during rested wakefulness predicts vulnerability to sleep deprivation. Neuroimage 111, 147–158.
Zhang, Y., Brady, M., Smith, S., 2001. Segmentation of brain MR images through a hidden Markov random field model and the expectation-maximization algorithm. IEEE Trans. Med. Imaging 20 (1), 45–57.
Zhu, Y., Cheng, L., He, N., Yang, Y., Ling, H., Ayaz, H., Tong, S., Sun, J., Fu, Y., 2017. Comparison of functional connectivity estimated from concatenated task-state data from block-design paradigm with that of continuous task. Comput. Math. Methods Med. 2017, 4198430.